Electronic Raman scattering in superconductors as a probe of anisotropic electron pairing

T. P. Devereaux
Department of Physics, University of California, Davis, California 95616

D. Einzel
Walther-Meissner-Institut für Tieftemperaturforschung, D-85748 Garching, Federal Republic of Germany
(Received 5 August 1994; revised manuscript received 23 January 1995)

A gauge-invariant theory for electronic Raman scattering for superconductors with anisotropic pairing symmetry is analyzed in detail. It is shown that Raman scattering in anisotropic superconductors provides a wealth of polarization-dependent information that probes the detailed angular dependence of the superconducting ground-state order parameter. The Raman spectra shows a unique polarization dependence for various anisotropic pair-state symmetries which affects the peak position of the spectra and generates symmetry-dependent low-frequency and temperature power laws that can be used to identify the magnitude and predominant symmetry of the energy gap. In particular, we calculate the collective modes and the subsequent symmetry-dependent Raman spectra for a $d_{x^2-y^2}$ superconductor and compare our results to the relevant data on the cuprate systems as well as theoretical predictions for s-wave, anisotropic s-wave, and mixed-state energy gaps. Favorable agreement is shown with the predictions for $d_{x^2-y^2}$ pairing and the experimental data on $YBa_2Cu_3O_7$, $Bi_2Sr_2CaCu_2O_8$, and $Tl_2Ba_2CuO_6$.

I. INTRODUCTION

Knowledge of the symmetry of the energy gap in superconductors provides a major step towards unraveling the puzzle of superconductivity in unconventional superconductors. While the evidence continues to accrue, the identification of the pair state in the heavy-fermion and cuprate systems has proven to be somewhat elusive.[1] While recent photoemission experiments[2] do allow for an angular-dependent determination of the gap and Josephson tunneling measurements have probed the phase of the gap,[3] by far the most abundant information that has led to speculation of a non-BCS ground state in high-T_c materials has been focused on the presence of power laws in the low-frequency and/or low-temperature behavior of transport and thermodynamic quantities.[4] However, due to the averaging over the entire Fermi surface, it is well known that the power laws themselves do not uniquely identify the ground-state symmetry of the order parameter but only can give the topology of the nodes of the energy gap along the Fermi surface, e.g., whether the gap vanishes on points and/or lines on the Fermi surface. Thus one cannot distinguish between different representations of the energy gap which have the same topology. For instance, for the case of d-wave tetragonal superconductors, there are five pure representations which have line nodes on the Fermi surface. Further, the energy gap can become smeared due to inelastic quasiparticle collisions, making a fully gapped superconductor seem like a one with gap nodes. While in principle the latter effect can be minimized by limiting the experiment to very low temperatures, the two-particle correlation functions determining the density, spin, or current response do not have the freedom to probe various portions of the gap around the Fermi surface, presenting a fundamental obstacle to uniquely identifying the pair-state representation for the superconductor.

However, it is well known that Raman scattering has the ability to measure various degrees of freedom by simply rotating the incident and scattered photon polarization orientations. Formally, Raman fluctuations may be viewed as anisotropic mass fluctuations around the Fermi surface which do not obey a conservation law,[5] such as, e.g., density fluctuations. While the long-wavelength density fluctuations between unit cells will be screened due to their coupling to long-range Coulomb forces, the intracell mass fluctuations can be anisotropic around the Fermi surface with no net charge and thus can be unscreened, providing a scattering mechanism for incoming photons.

Since the seminal work of Abrikosov and Fal'kovskii,[6] it is well known that superconductivity is manifest in Raman scattering via the opening of a gap for frequencies $\omega < 2\Delta$, with a ubiquitous BCS divergence at the gap edge. Indeed, quite a detailed theory exists for Raman scattering in s-wave superconductors, where the effects of Coulomb interactions,[7] small energy gap anisotropy,[8] final-state interactions,[9] and impurity scattering[10] have all been taken into account. However, the Raman spectra of unconventional superconductors with strongly $\mathbf{k}$-dependent energy gaps and nodes have only recently been addressed.[11,12] The presence of gap nodes leads to an incomplete reorganization of spectral intensity at low frequencies, and light scattering channels exist for all frequencies. Moreover, the question of gauge invariance, collective modes, and screening takes on a more important meaning due to excitons which can lie at much lower frequencies than in s-wave superconductors (as well as

0163-1829/95/51(22)/16336(22)/$06.00

possible additional spontaneously broken symmetries for certain gaps). This was brought to light in Ref. 11, which showed the delicate interplay of gauge modes and screening.

Most importantly, however, was the finding in Ref. 11 that a nontrivial coupling between the Raman vertex (to be specified later) and a strongly **k**-dependent energy gap leads to a rich polarization dependence of the spectra. Via this coupling, it was shown that crucial information can be obtained about the symmetry of the order parameter by analyzing the polarization dependence of the spectra. This is not the case for s-wave superconductors, where apart from a trivial multiplicative factor, a frequency-dependent polarization dependence is only seen in the vicinity of the gap edge (except for large impurity scattering).[9,10] In all previous studies, this coupling and its connection to polarization dependence was not explored. Therefore, we now review how the coupling of the vertex and energy gap arises.

The intensity of scattered light in a Raman experiment can be written in terms of a differential photon scattering cross section $\partial^2\sigma/\partial\omega\partial\Omega$ as

$$\frac{\partial^2\sigma}{\partial\omega\partial\Omega} = \frac{\omega_S}{\omega_I}\, r_0^2\, S_{\gamma\gamma}(\mathbf{q},\omega),$$
$$S_{\gamma\gamma}(\mathbf{q},\omega) = -\frac{1}{\pi}\,[1+n(\omega)]\,\mathrm{Im}\,\chi_{\gamma\gamma}(\mathbf{q},\omega). \tag{1}$$

Here $r_0 = e^2/mc^2$ is the Thompson radius, ω_I and ω_S are the frequency of the incoming and scattered photon, respectively, and we have set $\hbar = k_B = 1$. $S_{\gamma\gamma}$ is the generalized structure function, which is related to the imaginary part to the Raman response function $\chi_{\gamma\gamma}$ through the fluctuation-dissipation theorem, the second part of Eq. (1). The Raman response measures "effective density" fluctuations

$$\chi(\mathbf{q},\omega) = \langle[\tilde{\rho}(\mathbf{q}),\tilde{\rho}(-\mathbf{q})]\rangle_{(\omega)},$$

with

$$\tilde{\rho}(\mathbf{q}) = \sum_{\mathbf{k},\sigma}\gamma(\mathbf{k})c^\dagger_\sigma(\mathbf{k}+\mathbf{q})c_\sigma(\mathbf{k}).$$

The strength of the scattering is determined by the Raman vertex $\gamma(\mathbf{k})$. Finally $n(\omega)$ is the Bose-Einstein distribution function.

For small momentum transfers and incident light energies smaller than the optical band gap (nonresonant scattering), the vertex for Raman scattering can be written in terms of the curvature of the energy band dispersion $\epsilon(\mathbf{k})$,

$$\gamma(\mathbf{k}) = m\sum_{\alpha,\beta} e^S_\alpha \frac{\partial^2\epsilon(\mathbf{k})}{\partial k_\alpha \partial k_\beta} e^I_\beta, \tag{2}$$

where $\hat{\mathbf{e}}^{S,I}$ denote the scattered and incident polarization light vectors, respectively, which select elements of the Raman tensor. The symmetry of the underlying crystal can be taken into account by expanding γ in terms of a complete set of crystal harmonics Φ_L defined on the Fermi surface, i.e.,[13]

$$\gamma(\mathbf{k}) = \sum_{L,\mu}\gamma^\mu_L\Phi^\mu_L(\mathbf{k}), \tag{3}$$

where the index L represents the Lth-order contribution to the vertex which transforms according to the μth irreducible representation of the point group symmetry of the crystal. The quantum numbers L,μ classify the anisotropy of the Raman fluctuations around the Fermi surface. The full k dependence is thus described by the addition of the basis functions (which become progressively more anisotropic for higher L) with different weights γ^μ_L. While the charge, spin, and current density responses probe only a single L channel [$\gamma(\mathbf{k}) = 1$, $L = 0$, for the charge and spin density, while $\gamma(\mathbf{k}) = \mathbf{k}$, $L = 1$, for the current density], in principle all even L channels can contribute to the Raman vertex for bands which are nonparabolic. Thus by choosing the polarization light vectors accordingly, one can select different L,μ channels which allow for different projections onto the Fermi surface. By selecting fluctuations on different regions of the Fermi surface, light scattering can thus provide information on the strength of the pairing at different **k**-points along the Fermi surface. It is via this mechanism (the coupling of the vertex and energy gap) that the polarization dependence of the spectra can be used to determine the angular dependence of the pair-state symmetry.

In accordance with this fact, the experimental results on the cuprate systems reveal a wealth of polarization-dependent information that provides detailed evidence for determining the actual symmetry of the gap.[11] The existing body of data on the cuprate systems[14] reveals five main points: (1) In contrast to conventional superconductors such as Nb_3Sn, no clear well-defined gap is seen for any polarization orientation even at the lowest temperatures measured ($T/T_c = 0.03$),[15] (2) the peak of the spectrum lies roughly at 30% higher-frequency shifts for the polarization orientation which selects B_{1g} symmetry compared to all other symmetries,[14–22] (3) there are indications that the temperature dependence of the peak in the B_{1g} channel follows more closely a BCS form than any other symmetry,[19,21] (4) the low-frequency Raman shifts vary roughly as ω^3 for B_{1g} symmetries and linearly in ω for the others,[14–22] and (5) the ratio of residual scattering in the superconducting state to the normal state is smallest for the B_{1g} case compared to all other configurations.[20,21] Such a rich spectrum of information should provide a stringent test for various candidates of the pairing symmetry states.[23]

The purpose of the present paper is to investigate the polarization dependence of the Raman spectra for a superconductor in the weak-coupling limit with anisotropic pairing symmetry. We calculate the electronic Raman scattering for a tetragonal superconductor at finite temperatures and for various polarization orientations in a gauge-invariant manner and find a rich polarization dependence of the spectra that can be used to uniquely identify the predominant energy gap symmetry. Our calculations are restricted to charge fluctuations on the Fermi surface (this has the advantage that in some cases analytic solutions for response can then be obtained, but cannot account properly for the role of Van Hove sin-

gularities off the Fermi surface). In particular, we examine the Raman response for s-wave, d-wave, mixed-state, and anisotropic s-wave superconductors and find that a $d_{x^2-y^2}$ state agrees surprisingly well with the current information on electronic Raman scattering in $YBa_2Cu_3O_7$, $Bi_2Sr_2CaCu_2O_8$, and $Tl_2Ba_2CuO_6$.

The plan of the paper is as follows: The ground work for the gauge-invariant theory of electronic Raman scattering in anisotropic superconductors is reviewed in Sec. II using a kinetic equation approach; Sec. III concerns the connection of band structure to the Raman vertex; Sec. IV gives our results for the Raman response evaluated for four types of energy gaps, (i) s wave, (ii) d wave, (iii) mixed state, and (iv) one type of anisotropic s wave; Sec. V presents a comparison of the theory to the data on three cuprate systems and contains our conclusions. In Appendix A we discuss the connection between the Raman vertex and Fermi-surface harmonics expansions, and Appendix B deals with a solution of the weak-coupling gap equation for the case of anisotropic gaps, while Appendix C is devoted to our calculations for the massive collective modes and the subsequent role of vertex corrections using a diagrammatic approach. It is shown here how channel mixing, which occurs for anisotropic gaps and/or interactions, affects the Raman spectra.

II. KINETIC THEORY OF ELECTRONIC RAMAN SCATTERING IN ANISOTROPIC SUPERCONDUCTORS

A. Formalism

In this section we describe a kinetic equation approach for calculating generalized gauge-invariant response functions in anisotropic superconductors, with the majority of our attention being focused on the electronic Raman response. All previous calculations for the Raman response were carried out using a diagrammatic approach. The kinetic equation approach allows for a straightforward account of the Goldstone mode(s) for arbitrary pairing symmetry as well as the inclusion of Fermi-liquid interaction effects.

We consider an anisotropic superconductor in which the electronic states are characterized by a momentum $\mathbf{k}$, an energy (band) dispersion $\epsilon_k = \mu + \xi_k$ (with μ the Fermi energy), a (band) group velocity $\mathbf{v}_k = \nabla_k \epsilon_k$, an inverse effective mass tensor $M_{ij}^{-1}(\mathbf{k}) = \partial^2 \epsilon_k / \partial k_i \partial k_j$, an energy-gap Δ_k, and excitation energies $E_k = [\xi_k^2 + |\Delta_k|^2]^{1/2}$. In global thermodynamic equilibrium such a system is described by a diagonal equilibrium phase space distribution function n_k^0,

$$n_k^0 = \langle c_k^\dagger c_k \rangle = u_k^2 f(E_k) + v_k^2 [1 - f(E_k)] = \frac{1}{2}\left[1 - \xi_k \theta_k\right], \tag{4}$$

with $\theta_k = (1/2E_k)\tanh(E_k/2T)$, $f(E_k)$ the Fermi function taken at the Bogoliubov quasiparticle energy E_k, and the usual coherence factors $u_k^2 = \frac{1}{2}[1 + \xi_k/E_k]$ and $v_k^2 = \frac{1}{2}[1 - \xi_k/E_k]$ for particlelike and holelike Bogoliubov quasiparticles. In a superconductor there exists in addition to the diagonal average n_k^0 the off-diagonal average g_k^0,

$$g_k^0 = \langle c_{-k} c_k \rangle = -\Delta_k \theta_k. \tag{5}$$

The superconducting equilibrium energy gap is then determined from the self-consistency equation

$$\Delta_k = \sum_{\mathbf{p}} V_{kp}\, g_p^0, \tag{6}$$

with $V_{kp} = -|V_{kp}|$ the pairing interaction.

Such a system is assumed to be subject to external perturbation potentials $U_k^{\rm ext}(\mathbf{q},\omega) \propto \exp(i\mathbf{q}\cdot\mathbf{r} - i\omega t)$ which are generated in the usual way by an expansion of the Hamiltonian $\propto (\mathbf{p} - e\mathbf{A}^{\rm ext}/c)^2/2m + e\Phi^{\rm ext}$ containing $\mathbf{q}$- and ω-dependent scalar and vector electromagnetic potentials $\Phi^{\rm ext}(\mathbf{q},\omega)$ and $\mathbf{A}^{\rm ext}(\mathbf{q},\omega)$, respectively, to second order in the vector potential (including $\mathbf{p}\cdot\mathbf{A}$ terms):

$$\begin{aligned} U_k^{\rm ext} &= e\Phi^{\rm ext} + \mathbf{v}_k \cdot \left(-\frac{e}{c}\mathbf{A}^{\rm ext}\right) + \frac{e^2}{c^2}\, A_i^I M_{ij}^{-1}(\mathbf{k}) A_j^S, \\ &= e\Phi^{\rm ext} + \mathbf{v}_k \cdot \delta\vec{\epsilon}_1 + \gamma(\mathbf{k})\delta\epsilon_\gamma, \end{aligned} \tag{7}$$

where

$$\delta\vec{\epsilon}_1 = -\frac{e}{c}\mathbf{A}^{\rm ext},$$
$$\delta\epsilon_\gamma = r_0\, |\mathbf{A}^I|\, |\mathbf{A}^S|,$$

and $\gamma(\mathbf{k})$ denotes the Raman vertex given by Eq. (2). The last term in Eq. (7) can be interpreted to describe the scattering of an incident photon of frequency ω_I represented by the vector potential $\mathbf{A}^I$, into electronic excitations such as particle-hole, Bogoliubov quasiparticle, or magnon pairs and an outgoing photon (Stokes process) of frequency $\omega_S = \omega_I - \omega$ (vector potential $\mathbf{A}^S$) with an associated total momentum transfer $\mathbf{q}$.

The (linear) response of the distribution function $\delta n_k(\mathbf{q},\omega) = n_k(\mathbf{q},\omega) - n_k^0$ in the absence of dissipation is given by the solution of the collisionless (particle-hole-symmetric) kinetic equation[24,25]

$$\delta n_k = \frac{\eta_k}{\omega - \eta_k}(\phi_k - \lambda_k)\delta\epsilon_k - \lambda_k \delta\epsilon_k^+ + \lambda_k(\omega + \eta_k)\frac{\delta\Delta_k^-}{2|\Delta_k|}, \tag{8}$$

where $\eta_k \equiv \mathbf{v}_k \cdot \mathbf{q}$,

$$\phi_k = -\frac{\partial n_k^0}{\partial \xi_k} = \frac{|\Delta_k|^2}{E_k^2}\theta_k + \frac{\xi_k^2}{E_k^2}\varphi_k, \tag{9}$$

and $\varphi_k = -\partial f(E_k)/\partial E_k$. In addition we have defined

$$\delta\Delta_k^s = \frac{\delta\Delta_k \Delta_k^\dagger + s\Delta_k \delta\Delta_k^\dagger}{2|\Delta_k|}, \quad s = \pm 1. \tag{10}$$

The cases $s = -1$ and $s = +1$ distinguish the coupling of the response of the pair-correlated electron system to phase and amplitude fluctuations of the order parameter, respectively, and will be discussed later. The quantity λ_k is the pair response function introduced by Tsuneto[26] which, in the limit $q\xi \ll 1$, with ξ the coherence length, is given by

$$\lambda_k(\mathbf{q},\omega) = -4|\Delta_k|^2 \frac{(\omega^2-\eta_k^2)\theta_k + \eta_k^2\Phi_k}{\omega^2(\omega^2-4E_k^2) - \eta_k^2(\omega^2-4\xi_k^2)} \quad . \tag{11}$$

A more general expression for of λ_k valid also for $\xi^{-1} < q \ll k_F$ is given in Ref. 27. The total *diagonal* quasiparticle energy shift $\delta\epsilon_k = \delta\epsilon_k^+ + \delta\epsilon_k^-$ may be decomposed into the sum of contributions even (+) and odd (−) with respect to the parity operation $\mathbf{k} \to -\mathbf{k}$. It differs in general from the contribution from the external potential $U_k^{\rm ext}$ through vertex corrections or, more physically, through electronic polarization potentials.[28] This fact may be expressed through the diagonal self-consistency relation

$$\delta\epsilon_k = U_k^{\rm ext} + 2\sum_{\mathbf{p}}(V_q + f_{kp})\delta n_p. \tag{12}$$

Here, $V_q = 4\pi e^2/q^2$ is the Fourier transform of the long-range Coulomb interaction and f_{kp} denotes the short-range Fermi-liquid interaction, the consequences of which are, however, not considered in what follows since we are interested in the limit of not too large $\mathbf{q}$ where the polarization correction from the long-range Coulomb interaction dominates the diagonal energy change.

The kinetic equation for the linearized off-diagonal distribution function $\delta g_k(\mathbf{q},\omega) = g_k(\mathbf{q},\omega) - g_k^0$ reads

$$\delta g_k + \theta_k\delta\Delta_k + \frac{\omega^2-\eta_k^2}{4|\Delta_k|^2}\lambda_k\delta\Delta_k - \lambda_k\delta\Delta^\dagger\frac{\Delta_k}{|\Delta_k|} = \frac{\lambda_k}{2|\Delta_k|}\left[\omega\delta\epsilon_k^+ + \eta_k\delta\epsilon_k^-\right]. \tag{13}$$

A straightforward variation of the equilibrium gap equation (6) leads to an off-diagonal self-consistency relation

$$\delta\Delta_k(\mathbf{q},\omega) = \sum_{\mathbf{p}} V_{kp}\ \delta g_p(\mathbf{q},\omega), \tag{14}$$

which can now be used to compute the *off-diagonal* energy shifts, namely, the order parameter fluctuations $\delta\Delta_k(\mathbf{q},\omega)$ and $\delta\Delta_k^\dagger(-\mathbf{q},-\omega)$. They represent the collective oscillations necessary to maintain gauge invariance, and must be determined self-consistently with the off-diagonal kinetic equation[24,25] [from which particle-hole asymmetric terms, which are typically of the order $O(T/T_F)$, with T_F the Fermi temperature, have been omitted]

$$\sum_{\mathbf{p}} V_{kp}\lambda_p\frac{\omega^2-\eta_p^2}{4|\Delta_p|^2}\delta\Delta_p^- = \sum_{\mathbf{p}} V_{kp}\lambda_p\frac{\omega\delta\epsilon_p^+ + \eta_p\delta\epsilon_p^-}{2|\Delta_p|}. \tag{15}$$

In deriving (15) the equilibrium gap equation (6) has been used for simplification. In case of particle-hole symmetry, the density, current, and Raman fluctuations do not couple to the quantity $\delta\Delta^+$, which represents the amplitude fluctuations of the order parameter. The physical significance of the quantity $\delta\Delta_k^-$ becomes clear in the (macroscopic) limit $\omega \ll 2\Delta_0$, in which only fluctuations of the phase ϕ of the superconducting energy gap determine the dynamics of the condensate and $\delta\Delta_k^-(\mathbf{q},\omega) = |\Delta_k| i\delta\phi(\mathbf{q},\omega)$.

The important macroscopic observables, namely, the density fluctuations $\delta n_1(\mathbf{q},\omega)$, charge fluctuations $\delta n_e(\mathbf{q},\omega)$, the Raman fluctuations $\delta n_\gamma(\mathbf{q},\omega)$, and the current fluctuations $\mathbf{j}(\mathbf{q},\omega)$, are defined as

$$\begin{aligned}
\delta n_1(\mathbf{q},\omega) &= 2\sum_{\mathbf{k}} 1\ \delta n_k(\mathbf{q},\omega),\\
\delta n_e(\mathbf{q},\omega) &= 2\sum_{\mathbf{k}} e\ \delta n_k(\mathbf{q},\omega),\\
\delta n_\gamma(\mathbf{q},\omega) &= 2\sum_{\mathbf{k}} \gamma_k\delta n_k(\mathbf{q},\omega),\\
\mathbf{j}(\mathbf{q},\omega) &= 2\sum_{\mathbf{k}} \mathbf{v}_k[\delta n_k(\mathbf{q},\omega) + \phi_k\delta\epsilon_k(\mathbf{q},\omega)].
\end{aligned} \tag{16}$$

The factors of 2 arise from spin degeneracy.

We proceed with a solution of Eq. (15). For the time being we would like to restrict ourselves to the case where the pairing interaction factorizes as

$$V_{kp} = -V\frac{\Delta_k\Delta_p}{\Delta_0^2}. \tag{17}$$

This ansatz is sufficiently general to allow for an equilibrium gap function Δ_k of arbitrary anisotropy in $\mathbf{k}$ space. The maximum of such a gap is denoted Δ_0. Δ_k is determined from the following form for the equilibrium gap equation (see Appendix B for further details):

$$\frac{1}{V} = \sum_{p\in\text{shell}} \theta_p\frac{|\Delta_p|^2}{\Delta_0^2}. \tag{18}$$

Using Eq. (17), Eq. (15) can be solved immediately to give

$$\frac{\delta\Delta^-(\mathbf{q},\omega)}{2|\Delta_k|} = \frac{i}{2}\delta\phi(\mathbf{q},\omega) = \frac{\sum_{\mathbf{p}}\lambda_p(\omega\delta\epsilon_p^+ + \eta_p\delta\epsilon_p^-)}{\sum_{\mathbf{p}}\lambda_p(\omega^2-\eta_p^2)}. \tag{19}$$

The physical significance of the result (19) is that it describes the Goldstone mode for superconductors, the Anderson-Bogoliubov or gauge mode, i.e., the massless collective mode related to the spontaneously broken gauge symmetry. It is the existence of this mode which guarantees gauge invariance of the response theory or, equivalently, charge conservation, which we would like to briefly demonstrate now. For this purpose let us write the kinetic equation (8) in a form in which the left-hand side (lhs) is reminiscent of the usual Landau-Silin equation,[28]

$$\omega\delta n_k - \mathbf{q}\cdot\mathbf{v}_k\left[\delta n_k - \frac{\partial n_k^0}{\partial\xi_k}\delta\epsilon_k\right] = -\lambda_k[\omega\delta\epsilon_k^+ + \eta_k\delta\epsilon_k^-] + \lambda_k[\omega^2-\eta_k^2]\frac{\delta\Delta_k^-}{2|\Delta_k|}. \tag{20}$$

Inserting Eq. (19), one observes that the rhs of Eq. (20) vanishes upon summation over momenta $\mathbf{k}$ and the lhs of (20) generates the continuity equation for the particle number density,

$$\omega\delta n_1 - \mathbf{q}\cdot\mathbf{j} = 0. \tag{21}$$

Hence we have demonstrated that accounting properly for the fluctuations of the phase of the order parameter leads to the conservation law for the (charge) density. Alternatively, one could argue in the following way: The phase fluctuation term $\delta\Delta_k^-$ on the rhs of (20) can be thought of having its origin in a replacement of the scalar ($\Phi^{\rm ext}$) and vector ($\mathbf{A}^{\rm ext}$) potentials in the first term on the rhs of Eq. (20), representing the external potential contributions to $\delta\epsilon_k^+$ and $\delta\epsilon_k^-$, by their gauge-invariant counterparts

$$\begin{aligned}\Phi^{\rm ext} &\to \Phi^{\rm ext} - \frac{1}{c}\frac{\partial\chi}{\partial t},\\ \mathbf{A}^{\rm ext} &\to \mathbf{A}^{\rm ext} + \nabla\chi.\end{aligned} \tag{22}$$

The phase variable χ characterizing this gauge transformation can then be fixed by the requirement of charge conservation, which, together with the trivial connection between χ and the order parameter phase fluctuation $\delta\phi$,

$$\delta\phi = -\frac{2e}{c}\chi,$$

immediately leads to the result (19). This demonstrates clearly the equivalence of the existence of the Anderson-Bogoliubov mode with gauge invariance as well as the connection of gauge invariance with the conservation law for the (charge) density.

Next we would like to demonstrate two simple consequences of a gauge-invariant formulation of superconducting response theory, namely, those for the current response in the static ($\omega \to 0$) and for the Raman response in the homogeneous ($\mathbf{q} \to 0$) limit. The static limit of the kinetic equation (20) reads

$$\delta n_k - \frac{\partial n_k^0}{\partial\xi_k}\,\delta\epsilon_k = \lambda_k\delta\epsilon_k^- - \lambda_k\eta_k\frac{\sum_{\mathbf{p}}\lambda_p\eta_p\delta\epsilon_p^-}{\sum_{\mathbf{p}}\lambda_p\eta_p^2}. \tag{23}$$

Integrating this according to the prescription (16) one gets the static (super)current response expressed in a generalized London formula

$$\begin{aligned}\mathbf{j}_e(\mathbf{q},0) = e\mathbf{j}(\mathbf{q},0) &= -\frac{e^2}{c}\overleftrightarrow{\Delta}(\mathbf{q},0)\mathbf{A}^{\rm ext}(\mathbf{q},0),\\ \overleftrightarrow{\Delta}(\mathbf{q},\omega) &= \left\{\overleftrightarrow{\lambda} - \frac{\overleftrightarrow{\lambda}\cdot\mathbf{q}:\mathbf{q}\cdot\overleftrightarrow{\lambda}}{\mathbf{q}\cdot\overleftrightarrow{\lambda}\cdot\mathbf{q}}\right\}(\mathbf{q},\omega),\\ \overleftrightarrow{\lambda}(\mathbf{q},\omega) &= 2\sum_{\mathbf{p}}\lambda_p\,\mathbf{v}_p:\mathbf{v}_p.\end{aligned} \tag{24}$$

Clearly, the second term in (24), sometimes referred to as the backflow term,[29] is necessary to maintain charge conservation in the general case of an anisotropic superconductor. Equivalently, it guarantees that the current is purely transverse in the static limit.

Let us now turn to the Raman response in the homogeneous limit. Here we may ignore terms linear in $\Phi^{\rm ext}$ and $\mathbf{A}^{\rm ext}$. For $\mathbf{q} \to 0$ the kinetic equation (20) assumes then the strikingly simple form

$$\delta n_k = -\lambda_k\delta\epsilon_k^+ + \frac{\sum_{\mathbf{p}}\lambda_p\delta\epsilon_p^+}{\sum_{\mathbf{p}}\lambda_p}, \tag{25}$$

in which the second term on the rhs originates from the order parameter phase fluctuations. The Coulomb interaction becomes irrelevant in this limit, as will become clear later, and we may write $\delta\epsilon_k^+ = \gamma_k\delta\epsilon_\gamma$. The homogeneous Raman response of anisotropic superconductors can then be written in a form analogous to the London limit of the current response as

$$\begin{aligned}\delta n_\gamma(0,\omega) &= \Delta_{\gamma\gamma}(0,\omega)\delta\epsilon_\gamma(0,\omega),\\ \Delta_{ab}(\mathbf{q},\omega) &= -\left\{\lambda_{ab} - \frac{\lambda_{a1}\lambda_{1b}}{\lambda_{11}}\right\}(\mathbf{q},\omega),\\ \lambda_{ab}(\mathbf{q},\omega) &= 2\sum_{\mathbf{p}}\lambda_p\,a_pb_p,\quad a_p,b_p = 1,\gamma_p.\end{aligned} \tag{26}$$

As in the case of the current response there is a "backflow" term (the second term in the curly brackets), which guarantees charge conservation. This is easily seen in the limit of parabolic bands, where the Raman vertex γ_k is a constant and as a consequence the two terms in curly brackets cancel precisely. This is just another way of stating that there are no density fluctuations possible in the homogeneous limit $\mathbf{q} \to 0$ of a superconductor.

It is worth noting that there exists a homogeneous limit of the electronic Raman response also in normal metals when quasiparticle scattering processes are important characterized by a momentum-dependent lifetime τ_k. It is shown in Ref. 30 that an equation similar to (26) holds in the normal state with the Tsuneto function λ_k replaced by $\Lambda_k = (-\partial n_k^0/\partial\xi_k)(1 - i\omega\tau_k)^{-1}$.

Let us now turn to a description of the Raman response at finite wave vector $\mathbf{q}$. Our starting point will be Eq. (8) in which we select the even-parity contributions δn_k^+ and $\delta\epsilon_k^+ = \delta\epsilon_0 + \gamma_k\delta\epsilon_\gamma$ with $\delta\epsilon_0 = V_q\delta n_1$:

$$\begin{aligned}\delta n_k^+ &= [S_k + \Omega^2\lambda_k]\delta\epsilon_0 + \left[\gamma_k S_k + \Omega^2\lambda_k\frac{\lambda_{\gamma 1}}{\lambda_{11}}\right]\delta\epsilon_\gamma,\\ S_k &= \frac{\eta_k^2\phi_k - \omega^2\lambda_k}{\omega^2 - \eta_k^2},\\ \Omega^2 &= \frac{\omega^2}{\omega^2 - \omega_q^2},\quad \omega_q^2 = \frac{\mathbf{q}\cdot\overleftrightarrow{\lambda}\cdot\mathbf{q}}{\lambda_{11}}.\end{aligned} \tag{27}$$

Integration over momenta $\mathbf{k}$ in Eq. (27) yields equations that describe the coupling of density and Raman response:

$$\begin{aligned}\delta n_1 &= \chi_{11}^{(0)}\delta\epsilon_0 + \chi_{1\gamma}^{(0)}\delta\epsilon_\gamma,\\ \delta n_\gamma &= \chi_{\gamma 1}^{(0)}\delta\epsilon_0 + \chi_{\gamma\gamma}^{(0)}\delta\epsilon_\gamma,\end{aligned} \tag{28}$$

where we have defined the generalized (free) response functions

$$\begin{aligned}\chi_{ab}^{(0)} = \Delta_{ab} &+ \frac{\omega_q^2}{\omega^2 - \omega_q^2}\frac{\lambda_{a1}\lambda_{1b}}{\lambda_{11}}\\ &+ 2\sum_{\mathbf{p}}\left\{\frac{\eta_p^2(\phi_p - \lambda_p)}{\omega^2 - \eta_p^2}a_pb_p\right\}.\end{aligned} \tag{29}$$

The quantities $\chi^{(0)}_{ab}(\mathbf{q},\omega)$ are straightforward generalizations of the free superconducting Lindhard function which include vertices a_k, b_k. The Anderson-Bogoliubov collective mode causes the second term in the transverse contribution Δ_{ab} (note that $\Delta_{a1}=\Delta_{1b}=\Delta_{11}\equiv 0$) and the longitudinal term which is characterized by the gauge mode frequency ω_q. Finally we explicitly work out the Coulomb renormalization $\delta\epsilon_0 = V_q\delta n_1$ which couples Raman and density fluctuations and arrive at the following final result:

$$\begin{aligned}\delta n_\gamma &= \chi_{\gamma\gamma}\delta\epsilon_\gamma,\\ \chi_{ab} &= \chi^{(0)}_{ab} - \frac{\chi^{(0)}_{a1}\chi^{(0)}_{1b}}{\chi^{(0)}_{11}} + \frac{\chi^{(0)}_{a1}\chi^{(0)}_{1b}}{\chi^{(0)}_{11}}\frac{1}{\epsilon},\\ \epsilon &= 1 - V_q\chi^{(0)}_{11}.\end{aligned} \tag{30}$$

It should be noted that the Raman response in superconductors in the small-q limit in a form equivalent to Eq. (30) was derived by Klein and Dierker[8] using the Green's-function method. Our result from the kinetic equation method looks slightly different and, particularly, one can see that the Coulomb interaction acts so as to split the Raman response into an unscreened "transverse" and a dielectrically screened "longitudinal" part, the latter being described by the full dielectric function of $\epsilon(\mathbf{q},\omega)$ of the superconductor in complete analogy to the behavior of the current response, discussed in Ref. 29. Furthermore, an inspection of Eq. (30) shows that all terms in the full response function χ_{ab} except $\Delta_{\gamma\gamma}$ are at least of the order $O(q^2)$, the last (longitudinal) term being even smaller, of the order $O(q^2/\epsilon)$. The role of the Coulomb interaction is thus limited to show up in terms of the order of at most $O(q^2)$ and is seen to be negligible in the homogeneous limit. The role of the collective Anderson-Bogoliubov mode, on the other hand, mainly consists of providing a particle number conservation law. This manifests itself first in the correct mass fluctuation limit of Eq. (30), in which γ_k=const and all transverse terms vanish identically leaving essentially the screened random-phase-approximation (RPA) Lindhard response of the superconductor in which the collective mode gets shifted to the plasma frequency. Second it manifests itself in "partial screening" effects in the homogeneous limit of the Raman response, described by the second term of $\Delta_{\gamma\gamma}$. These effects will be discussed in detail later.

B. Final results for $\mathbf{q}\to 0$

Since $q\xi \ll 1$ in the cuprates (with ξ the coherence length), we are mostly interested in Raman scattering with vanishing momentum transfers. For such a case it is essential to conclude at this stage that the most important contribution to the electronic Raman effect in superconductors in the small-$\mathbf{q}$ collisionless limit comes from the response function $\Delta_{\gamma\gamma}(0,\omega) = \lim_{\mathbf{q}\to 0}\chi_{\gamma\gamma}(\mathbf{q},\omega)$. Physically, this function describes the photon-induced breaking of a Cooper pair into a pair of Bogoliubov quasiparticles with total momentum $\mathbf{q}$ which is approximately zero.

Writing the Raman vertex γ as a sum $\gamma(\mathbf{k}) = \gamma_0 + \delta\gamma(\mathbf{k})$ of an isotropic and an anisotropic part [using Fermi-surface harmonics $\delta\gamma(\mathbf{k}) = \sum_{L\neq 0}\gamma_L(\mathbf{k})$], one may decompose the screened Raman response function at zero temperature in the limit of small momentum transfers as $\chi_{\gamma\gamma} = \chi_{\|} + \chi_{\perp}$, with

$$\begin{aligned}\chi_{\|} &= \frac{[\chi^{(0)}_{\gamma 1}]^2}{\chi^{(0)}_{11}}\frac{1}{\epsilon} = O\left(\frac{q^2}{\epsilon}\right),\\ \chi_{\perp} &= \Delta_{\delta\gamma\delta\gamma}(0,\omega) + O(q^2),\end{aligned} \tag{31}$$

into a longitudinal part ($\|$), affected by (longitudinal) screening through the dielectric function ϵ of the superconductor, and a transverse part ($\perp$), independent of ϵ. Thus for $\mathbf{q}\to 0$, only the transverse part of χ remains. We also see that in the case of the isotropic density vertex $\gamma(\mathbf{k}) = \gamma_0$, the long-range Coulomb forces completely screen the response and thus the only contribution to Raman scattering at $q = 0$ comes from energy bands with nonparabolic dispersion, i.e., the $L = 2$ and higher terms, representing intracell charge fluctuations.

Taking the limit of $\mathbf{q}\to 0$ and carrying out the ξ integration in the Tsuneto function, we obtain the final result for the Raman response at finite temperatures,

$$\chi(\mathbf{q}\to 0, i\omega) = \chi_{\delta\gamma,\delta\gamma}(i\omega) - \frac{\chi^2_{\delta\gamma,1}(i\omega)}{\chi_{1,1}(i\omega)}, \tag{32}$$

where the spectrum of $\chi_{a,b}$ is given by

$$\chi''_{a,b}(\omega) = \frac{\pi N_F}{\omega}\tanh\left(\frac{\omega}{4T}\right)\mathrm{Re}\left\langle\frac{a(\mathbf{k})b(\mathbf{k})\mid\Delta(\mathbf{k})\mid^2}{\sqrt{\omega^2-4\mid\Delta(\mathbf{k})\mid^2}}\right\rangle, \tag{33}$$

where N_F is the density of states for both spin projections, Re denotes taking the real part, and $\langle\cdots\rangle$ denotes performing an average over the Fermi surface defined by

$$\langle A(\mathbf{k})\rangle = \frac{\int d^2k\,\delta(E_F-\epsilon(\mathbf{k}))A(\mathbf{k})}{\int d^2k\,\delta(E_F-\epsilon(\mathbf{k}))}.$$

The real part of χ is given for $T = 0$ as

$$\chi'_{a,b}(\omega) = \langle a(\mathbf{k})b(\mathbf{k})A'(\omega)\rangle, \tag{34}$$

$$A'(\omega) = N_F\frac{\mid\Delta(\mathbf{k})\mid^2}{\omega}\begin{cases}\frac{2}{\sqrt{\mid\Delta(\mathbf{k})\mid^2-(\omega/2)^2}}\arctan\left(\frac{\omega}{2\sqrt{\mid\Delta(\mathbf{k})\mid^2-(\omega/2)^2}}\right), & \mid\Delta(\mathbf{k})\mid^2 > (\omega/2)^2,\\ \frac{1}{\sqrt{(\omega/2)^2-\mid\Delta(\mathbf{k})\mid^2}}\ln\left[\frac{\omega/2-\sqrt{(\omega/2)^2-\mid\Delta(\mathbf{k})\mid^2}}{\omega/2+\sqrt{(\omega/2)^2-\mid\Delta(\mathbf{k})\mid^2}}\right], & \mid\Delta(\mathbf{k})\mid^2 \le (\omega/2)^2.\end{cases}$$

This is the expression for the gauge-invariant Raman response which has Coulomb screening and the Anderson-Bogoliubov gauge mode taken into account. It is also the form for the response calculated diagrammatically in the "pair approximation" for the bare bubble, modified with the usual RPA screening terms.[7] It does not take into account any vertex corrections resulting from the pairing interaction in other channels other than the pairing channel, as explained in the preceding discussion. We will refer back to these expressions in the following sections.

Important information can also be obtained from the temperature dependence of the response in the limit of zero-frequency shifts, i.e., the static response. It can be shown that the ratio of the response in a superconductor to that of a normal metal in the limit of vanishing frequencies is given by the simple expression

$$\frac{\chi''_{\rm sc}(\omega \to 0)}{\chi''_{\rm ns}(\omega \to 0)} = \frac{2\langle f(\mid \Delta(\hat{\mathbf{k}}) \mid) \mid \delta\gamma(\hat{\mathbf{k}}) \mid^2\rangle}{\langle \mid \delta\gamma(\hat{\mathbf{k}}) \mid^2\rangle}, \tag{35}$$

where f is a Fermi function.[10] This is an exact result which does not depend on vertex corrections and only depends appreciably on impurity scattering for nearly resonant impurity scatterers.[10,31]

The important feature in all these expressions is that in general a coupling of the Raman vertex to the energy gap can occur under the momentum averaging over the Fermi surface. In all previous studies, this k dependence was either ignored or not fully exploited to determine important information concerning the symmetry of the energy gap. This will be explicitly demonstrated in the following section where we evaluate these expressions for the screened Raman response for various pair-state candidates and discuss its relevance to the cuprate materials.

We close this section by returning to the question of the presence of massive modes and final-state vertex corrections (see above). In principle, the massive modes can lie at low frequencies and affect the low-frequency behavior of correlation functions and, in particular, could even be used as a signal for a certain type of order parameter symmetry. We have carried out an analysis of the full gauge-invariant calculation in Appendix C for both cylindrical and spherical Fermi surfaces for a generalized pairing interaction. We identified the position of the collective modes as a function of coupling strength for a gap of $d_{x^2-y^2}$ (Γ_3^+ representation using the notation of Sigrist and Rice[32]) symmetry for both a spherical and cylindrical Fermi surface. Our conclusions are threefold: (1) The Goldstone modes do affect the Raman spectrum in the limit of $\mathbf{q} \to 0$, in certain polarization symmetries (A_{1g}) where the backflow term in (32) is finite, (2) optical (massive) collective modes couple to a light probe only for the case of a Fermi surface with z dispersion for d-wave vertex corrections in the B_{1g} and E_g channels, and (3) these modes are significantly damped and have a vanishing residue for those modes which lie at low energies. Therefore, the collective modes are of little importance to the Raman spectrum. These conclusions can be generalized to other energy gaps which have line nodes on the Fermi surface. Also, we discuss the role of the final-state interactions and find that while the overall shape of the spectra can be affected, the corrections are relatively minor. The details are contained in Appendix C, including a more general discussion of the role of vertex corrections. Therefore, we can conclude that Eqs. (32)–(35) give an adequate description of the Raman response.

III. BAND STRUCTURE, FERMI SURFACE, AND THE RAMAN VERTEX FOR TETRAGONAL SYMMETRY

In this section we aim at providing a link between the Raman vertex and band structure for tetragonal crystals. In particular, we show how the choice of light polarization orientations results in selection rules for the symmetry components of the Raman tensor. In the first subsection we only consider scattering within a single band while we consider the case of multiple bands at the Fermi surface in the following subsection.

A. Single band

As we have seen in the previous section [see Eq. (2)], the Raman tensor is directly related to the curvature of the band dispersion. In the following we limit our considerations to tetragonal materials which are relevant to high-T_c superconductors. Although these materials possess orthorhombic distortions away from tetragonality, the selection rules, for example, from phonon scattering in the normal state seem to indicate that these orthorhombic distortions are small and that a tetragonal symmetry classification can be employed with little loss of generality. A simplest choice for the band structure which contains the basic physics of two-dimensional- (2D-) like tetragonal systems with lattice constant a is given by

$$\epsilon(\mathbf{k}) = -2t\,[\cos(k_x a) + \cos(k_y a)] + 4t' \cos(k_x a)\cos(k_y a). \tag{36}$$

Here t and t' are the nearest and next nearest neighbor hopping parameters, respectively. This is the antibonding band derived from a reduction of a three-band model,[33] which gives a large contribution to the density of states at the Fermi level for the cuprate systems and adequately reproduces the observed photoemission data.[2,33,34]

The Raman tensor is given by

$$\overleftrightarrow{\gamma}(\hat{\mathbf{k}}) = mM^{-1}(\hat{\mathbf{k}}) = 2ma^2 \begin{pmatrix} t[f_k^{(0)} + f_k^{(3)}] + t' f_k^{(0)\prime} & t' f_k^{(1)} \\ t' f_k^{(1)} & t[f_k^{(0)} - f_k^{(3)}] + t' f_k^{(0)\prime} \end{pmatrix}, \tag{37}$$

where $M^{-1}_{\alpha\beta} = \partial^2\epsilon(\mathbf{k})/\partial k_\alpha \partial k_\beta$, and $f_k^{(\nu)}$ is defined as

$$f_k^{(0)} = \frac{1}{2}[\cos(k_x a) + \cos(k_y a)], \quad f_k^{(3)} = \frac{1}{2}[\cos(k_x a) - \cos(k_y a)],$$
$$f_k^{(0)\prime} = -2\cos(k_x a)\cos(k_y a), \quad f_k^{(1)} = 2\sin(k_x a)\sin(k_y a). \tag{38}$$

We proceed to expand the Raman tensor in quarternions,

$$\overleftrightarrow{\gamma}_k = m\overleftrightarrow{M}^{-1} = \sum_{\mu=0}^{3} \gamma_k^{(\mu)}\, \tau^\mu, \tag{39}$$

with τ^μ the Pauli matrices in 2D $\mathbf{k}$ space. This expansion in the space of 2×2 matrices decomposes the Raman tensor into its symmetry components, represented by the scalar coefficients γ_k^μ,[35]

$$\gamma_k^\mu = \begin{cases} 2ma^2[tf_k^{(0)} + t'f_k^{(0)\prime}], & A_{1g}\ (\mu = 0), \\ 2ma^2 t' f_k^{(1)}, & B_{2g}\ (\mu = 1), \\ 2ma^2 t f_k^{(3)}, & B_{1g}\ (\mu = 3). \end{cases} \tag{40}$$

The polarization light vectors select elements of the Raman tensor according to

$$\gamma_k^{IS} = \hat{e}^I \overleftrightarrow{\gamma}_k \hat{e}^S = \sum_\mu (\hat{e}^I \tau^\mu \hat{e}^S)\, \gamma_k^\mu. \tag{41}$$

A few examples of the connection between polarization and symmetry are

$$\gamma_k^{xx} = \gamma_k^{(0)} + \gamma_k^{(3)}, \quad \gamma_k^{yy} = \gamma_k^{(0)} - \gamma_k^{(3)},$$
$$\gamma_k^{xy} = \gamma_k^{yx} = \gamma_k^{(1)}, \quad \gamma_k^{x'y'} = \frac{1}{2}[\gamma_k^{xx} - \gamma_k^{yy}] = \gamma_k^{(3)},$$
$$\gamma_k^{x'x'} = \frac{1}{2}[\gamma_k^{xx} + \gamma_k^{yy} + 2\gamma_k^{xy}] = \gamma_k^{(0)} + \gamma_k^{(1)}, \tag{42}$$
$$\gamma_k^{y'y'} = \frac{1}{2}[\gamma_k^{xx} + \gamma_k^{yy} - 2\gamma_k^{xy}] = \gamma_k^{(0)} - \gamma_k^{(1)},$$

where $x' = \frac{1}{\sqrt{2}}[x+y]$ and $y' = \frac{1}{\sqrt{2}}[x-y]$. These examples show in particular that A_{1g} symmetry cannot be individually accessed for in-plane polarizations, and subtraction procedures must be used.

B. Multisheeted Fermi surfaces

We close this section with a discussion concerning scattering from the antibonding band to another band near or at the Fermi level. Recently it has been suggested that scattering from either the antibonding plane band to the other plane band or a chain band is important in the cuprates.[36] However, this seems to be in contradiction to the results obtained on Y-Ba-Cu-O,[18,16] Bi-Sr-Ca-Cu-O,[19] single-,[20] double-,[22] and triple-layer thallium cuprate,[21] and La cuprate[17] compounds. These compounds, all with different band structures, chains, and number of planes, all show qualitatively the same polarization-dependent Raman spectra. This is unexpected if multiband scattering were indeed important.

The above consideration can be easily adopted to the case of multiple energy bands contributing to the Fermi surface, for instance, due to the contribution of the chains (in Y-Ba-Cu-O) as well as the planes.[37,38] For intracell fluctuations, the total electronic Raman cross section for intraband scattering is just the sum of the contribution to the cross section for each band and thus results from the addition of the Raman response functions

$$\chi_{\text{total}} = \sum_\alpha \chi_\alpha\{\Delta_\alpha\}, \tag{43}$$

where $\chi_\alpha\{\Delta_\alpha\}$ denotes the contribution to the scattering from band α with an energy gap Δ_α for each band. The Raman vertex for each band is separately calculable in the same manner as in the previous section, and the same considerations there can be carried over to the multisheeted case trivially. This holds only for the B_{1g} and B_{2g} channels, which solely represent intracell charge fluctuations. Since the A_{1g} channel contains intercell charge fluctuations as well, light scattering can mix intercell fluctuations on different bands, leading to the appearance of an additional mixing term to Eq. (44).[36,38] This term has been shown to be small for the case of nearly degenerate bands, while for the case of degenerate bands, the mixing term can be shown to vanish.[37,38] Thus, for nearly degenerate bands, the response is well approximated by the addition of the result for each single band. The consequences of many bands will be further considered in a forthcoming publication.[38]

We draw the important point, however, that the contribution from each band will be weighted by the relative density of states and curvature of each band at the Fermi level. Therefore, for the case of the cuprates we believe that the largest contribution to electronic Raman scattering is thus arising from the single antibonding Cu-O layer band with the largest density of states and greatest curvature at the Fermi level. Therefore, we feel that, to a very good approximation, the intraband scattering has a dominant contribution from the antibonding band. This is certainly the case for the single Cu-O layer compounds $Tl_2Ba_2CuO_6$ and $La_{2-x}Sr_xCuO_4$.

IV. PREDICTIONS FOR VARIOUS PAIR STATES

In this section we evaluate Eqs. (32) and (33) for various pair states that are discussed in the literature as candidates to describe the pairing symmetry in the cuprates. We will first discuss the simple case of an isotropic gap and then discuss d-wave gaps (in particular, we will focus on the $d_{x^2-y^2}$ pairing symmetry). Last, we also discuss gaps which are anisotropic but do not contain nodes, e.g., a gap with mixed states, and an anisotropic s-wave gap.

A. Isotropic s-wave gap

For the case of an angular-independent gap $\Delta(\mathbf{k}) = \Delta_0$, the Raman response is given by the simple BCS

expression. It has the stereotypic features of BCS theory, namely, the existence of an energy gap threshold 2Δ required to break a Cooper pair, and the ubiquitous square root divergence associated with the gap edge. We note in particular that the Raman vertex couples trivially to the energy gap and just determines an overall prefactor governing the Raman intensity. The vertex does not affect the line shape and thus the line shape is polarization independent. A polarization dependence can be generated in BCS theory by taking into account channel-dependent final-state interactions[9] and/or impurity scattering,[10] and accurate fits to the Raman data on $A15$ superconductors can be obtained. However, for the most part this only produces a channel dependence in the vicinity of the gap edge and thus the main feature of the response is the uniform gap existing for all polarizations, which clearly cannot give an adequate description of the Raman spectra of the cuprate materials.

B. $d_{x^2-y^2}$ pairing

The explicit symmetry dependence of the spectra results due to a coupling of the energy gap and vertex when the energy gap is anisotropic. In order to proceed with the evaluation of Eq. (33) using the vertices derived in Sec. III, we make the following approximations in order to simplify the calculations. We first approximate the Fermi surface as being a cylinder. This leads to the unfortunate result that the subsequently derived Raman vertices are zero after screening, and thus yield no Raman signal. Therefore we must allow for deviations away from cylindricity when calculating the vertices. This can be done in general by expanding the vertices in terms of Fermi-surface harmonics depending on azimuthal angle φ. Retaining only the first nonvanishing term of the vertices in a Fermi-surface harmonic expansion we obtain

$$\gamma_k^{B_{1g}} = \gamma_{B_{1g}} \cos(2\varphi), \quad \gamma_k^{B_{2g}} = \gamma_{B_{2g}} \sin(2\varphi), \tag{44}$$

$$\gamma_k^{A_{1g}} = \gamma_0 + \gamma_{A_{1g}} \cos(4\varphi).$$

The coefficients of the expansion γ contain details of the shape of the Fermi surface and thus will be taken as a parameter to be fit to the data. This only controls the overall intensity of the spectra and has no effect on the line shape (this is not serious since often the experimental data are presented in arbitrary units). While not consistent, these approximations do capture the channel dependence of the Raman spectra, which is mainly determined by the nodal topology of the vertex and the gap in the Fermi-surface average in Eq. (33) (e.g., the manifold that the functions are averaged on does not crucially affect the results). These approximations are discussed in Appendix A, where we refer the reader for technical details. Last, in order to check the accuracy of our approximations, we will evaluate the Raman spectra using the Fermi surface and vertices derived from the t-t' band structure of Sec. III A. We find only minor differences, which validates our expansion.

Using a $d_{x^2-y^2}$ gap $\Delta(\hat{\mathbf{k}}, T) = \Delta_0(T)\cos(2\varphi)$ (see Appendix B), we find that the Raman spectrum can be written down analytically in terms of complete elliptical integrals. Taking screening into account and defining $x = \omega/2\Delta_0$, we obtain, for $T = 0$,

$$\chi''^{\,\mathrm{sc}}_{B_{1g}} = \chi''_{B_{1g}}(\mathbf{q}=0,\omega) = \frac{2N_F\gamma^2_{B_{1g}}}{3\pi x} \times \begin{cases} [(2+x^2)K(x) - 2(1+x^2)E(x)], & x \le 1\ , \\ x[(1+2x^2)K(1/x) - 2(1+x^2)E(1/x)], & x > 1, \end{cases} \tag{45}$$

$$\chi''^{\,\mathrm{sc}}_{B_{2g}} = \chi''_{B_{2g}}(\mathbf{q}=0,\omega) = \frac{2N_F\gamma^2_{B_{2g}}}{3\pi x} \times \begin{cases} [(1-x^2)K(x) - (1-2x^2)E(x)], & x \le 1\ , \\ x[(2-2x^2)K(1/x) - (1-2x^2)E(1/x)], & x > 1; \end{cases} \tag{46}$$

i.e., the B_{1g} and B_{2g} channels are not affected by transverse screening and the gauge mode. This is consistent with the mass fluctuations being only intracell in nature for these symmetry channels. However, the A_{1g} channel which contains both intercell and intracell fluctuations is partially screened and is determined via

$$\chi^{\mathrm{sc}}_{A_{1g}}(i\omega) = \chi_{A_{1g},A_{1g}}(i\omega) - \frac{\chi^2_{A_{1g},1}(i\omega)}{\chi_{1,1}(i\omega)}, \tag{47}$$

with the spectral functions

$$\chi''_{A_{1g},A_{1g}}(\mathbf{q}=0,\omega) = \frac{2N_F\gamma^2_{A_{1g}}}{15\pi x} \times \begin{cases} [(7-8x^2+16x^4)K(x) - (7-12x^2+32x^4)E(x)], & x \le 1, \\ x[(11-28x^2+32x^4)K(1/x) - (7-12x^2+32x^4)E(1/x)], & x > 1, \end{cases} \tag{48}$$

$$\chi''_{A_{1g},1}(\mathbf{q}=0,\omega) = \frac{\sqrt{2}N_F\gamma_{A_{1g}}}{3\pi x} \times \begin{cases} [(1+2x^2)K(x) - (1+4x^2)E(x)], & x \le 1, \\ x[(-1+4x^2)K(1/x) - (1+4x^2)E(1/x)], & x > 1, \end{cases} \tag{49}$$

and

$$\chi''_{1,1}(\mathbf{q}=0,\omega) = \frac{N_F}{\pi x} \times \begin{cases} [K(x) - E(x)], & x \le 1, \\ x[K(1/x) - E(1/x)], & x > 1. \end{cases} \tag{50}$$

The real parts are obtainable through Kramers-Kronig transformation or numerically integrating Eq. (34). The response functions for finite T are obtained simply by multiplying Eqs. (45)–(50) by the factor $\tanh(\omega/4T)$. The partial screening of the A_{1g} channel arises techni-

cally from the observation that the square of the energy gap enters into the response function in Eq. (33). For the case of $d_{x^2-y^2}$ pairing symmetry, the energy gap squared contains a term which transforms according to A_{1g} symmetry which leads to a finite overlap with the A_{1g} vertex in Eq. (32). This corresponds to partial "transverse screening" of the A_{1g} channel, and via this mechanism the intercell fluctuations are removed. Similar considerations hold if the gap were of another d-wave symmetry other than $d_{x^2-y^2}$.

These functions are plotted in Fig. 1(a) for the three symmetries indicated. We immediately see that the spectra are extremely polarization dependent, in contrast to the case of isotropic s-wave superconductors which are dominated by the square root divergence at the threshold in each channel. We see that the peak in the Raman spectra lies at different frequencies $\omega_{\mathrm{peak}} \sim 2\Delta_0(T), 1.6\Delta_0(T)$, and $1.2\Delta_0(T)$ for the B_{1g}, B_{2g}, and A_{1g} channels, respectively.[40] The symmetry dependence of the spectra is a direct consequence of the angular averaging which couples the gap and Raman vertex, and leads to constructive (destructive) interference under averaging if the vertex and the gap have the same (different) symmetry. Thus it has been reasoned that the symmetry which shows the highest peak position gives a unique indication of the predominant symmetry of the gap.[11] The peak positions can be mildly affected by including interaction vertex corrections as discussed in Appendix C, with the net result being a slight upward shift of the peak location in the B_{2g} and A_{1g} channels. Also, while the presence of z dispersion has little effect on the B_{1g} (apart from cutting off the logarithmic divergence) and B_{2g} channels, the A_{1g} peak position can be changed due to the addition of a term which has its main contribution at slightly lower frequencies. This effect is small provided that the Fermi surface is mostly cylindrical. We refer the reader to Appendix C for details.

The symmetry dependence is also manifest in the low-frequency behavior, which can be written as

$$\begin{aligned}
\chi''_{B_{1g}}(\omega \to 0) &= 3N_F\gamma^2_{B_{1g}}x^3/4 + O(x^5), \\
\chi''_{B_{2g}}(\omega \to 0) &= N_F\gamma^2_{B_{2g}}x/2 + O(x^3), \\
\chi''_{A_{1g}}(\omega \to 0) &= N_F\gamma^2_{A_{1g}}x/2 + O(x^3);
\end{aligned} \tag{51}$$

i.e., the spectrum rises slower in the B_{1g} channel than the A_{1g} or B_{2g} channels, which have the same linear rise with frequency. The power laws are insensitive to vertex corrections and arise solely due to topology arguments. The appearance of power laws is a signature of an energy gap which vanishes on lines (points in 2D) on the Fermi surface. However, the channel dependence of the exponents is unique to a $d_{x^2-y^2}$ pair state. These channel-dependent power laws have been observed in the electronic contribution to Raman scattering in Bi-Sr-Ca-Cu-O,[11,19] Y-BaCu-O,[18,16] Tl-Ba-Cu-O,[20,22,21] and La 214,[17] and are strong evidence for a d-wave gap of this symmetry as opposed to d_{xy}, d_{xz}, or d_{yz} symmetry, which also have nodes on lines on the Fermi surface.[11,40]

Of course a nearly cylindrical system is a simplification of real systems and ignores additional physics of Van Hove singularities and nesting peculiar to 2D systems. However, we expect only small changes in the response due to a change in the shape of the underlying manifold. To check this, we have redone the averages in Eq. (33) numerically using a Fermi surface given by the band structure, Eq. (36). Our results for the channel-dependent spectra are given in Fig. 1(b), using the parameters $2t'/t = 1.3$ and $\mu/2t = -0.5$ appropriate for dopings which produce the highest T_c values.[39] We have also performed the calculations for a Fermi surface which is more square like ($\mu/2t = -0.2$, $2t'/t = 0.01$) and obtain qualitatively the same results shown in Fig. 1(b). We immediately see that the low-frequency power-law behavior of the spectra is unchanged while the peak positions shift only slightly downward (less than 10%) with respect to those obtained for the approximations of retaining only leading-order Fermi-surface harmonics. We again remark that the same order of an effect in the opposite direction is seen when final-state interactions are taken into account (see Appendix C), which would reduce the effects of deviations from cylindricity of the Fermi surface. The intensity scales with the hopping parameter t for the B_{1g} channel, and with t' for the B_{2g} and A_{1g} channels. These result thus support the argument that

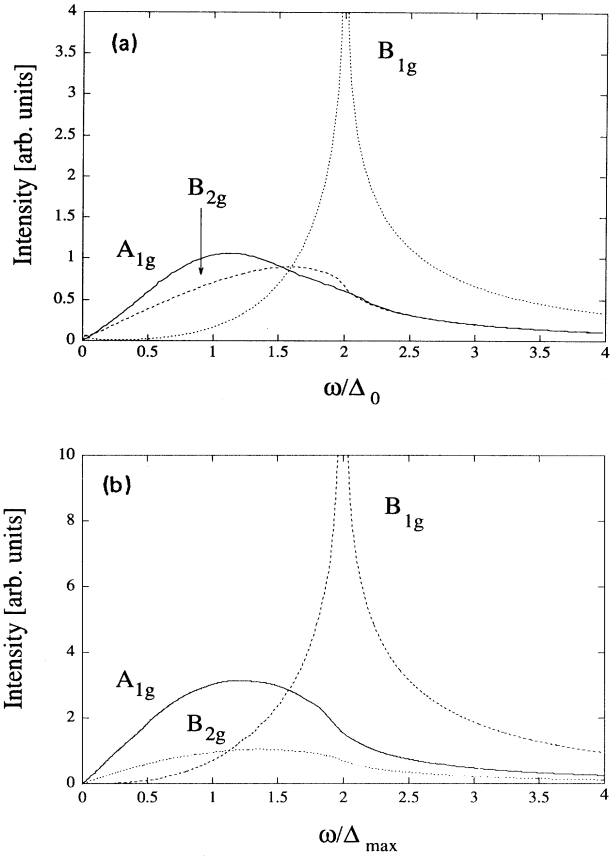

FIG. 1. (a) Electronic Raman response functions evaluated for $d_{x^2-y^2}$ pairing on a cylindrical Fermi surface for various symmetries as indicated. All vertices have been set equal to 1. (b) Electronic Raman response functions evaluated for Fermi surface derived from band structure of Eq. (36), with the parameters $\mu/2t = -0.5$, $2t'/t = 1.3$.

the line shape of the spectra is solely governed by the coupling of the vertex and energy gap, and is thus relatively insensitive to the topology of the Fermi surface. Therefore, for the purposes of obtaining the line shape we will restrict ourselves to the approximations leading to Eq. (44). We do note that part of the Van Hove singularities [for instance, at $(\pi,0)$] cannot be picked up directly using Eq. (33) and a full $\mathbf{k}$ sum must be performed using the band specific Green's function. However, it is expected that finite $\mathbf{z}$ dispersion and impurity and/or inelastic scattering will limit the role of Van Hove effects. This remains to be explored.

We now investigate the temperature dependence of the theory and contrast it to that of an isotropic s-wave superconductor. Using a weak-coupling expression for the temperature dependence of the energy gap $(2\Delta_0/T_c = 4.2794)$ (see Appendix B), we numerically evaluate Eq. (35) for the temperature dependence of the normalized static response while taking screening into account. This function describes how the gap in the Raman spectrum at low energies opens up with cooling below T_c. The results are plotted in Fig. 2 as a function of T/T_c for a $d_{x^2-y^2}$ energy gap compared to a BCS isotropic gap. The low-temperature behavior is given by a power law in T for all channels for the d-wave case while the ubiquitous exponential dependence in T is seen for all channels in the s-wave case. The power-law behavior for the d-wave case is channel dependent, with exponents identical to those of Eq. (51), in the sense that ω can be replaced by T. What is remarkable is that the falloff of the Fermi function at low temperatures is quite slow in those channels which are orthogonal to the symmetry of the gap, where the A_{1g} and B_{2g} channels show a residual broadening at $T/T_c = 0.3$ of roughly 20% of that of the normal state. This was argued in the case of electronic Raman scattering to be further evidence for an energy gap in the cuprate materials which has predominantly $|B_{1g}|$ character, due to the observation that a gap opens up quickly in the B_{1g} channel compared to other channels which have been probed via Raman scattering.[11]

As we have remarked before, since the Raman density response function (in the absence of impurity scattering[31]) only depends on the magnitude of the energy gap, it cannot be sensitive to the phase of the order parameter and thus cannot be directly used to determine if the gap changes sign around the Fermi surface. While the power-law behavior at low frequencies and/or temperatures is indicative of the presence of nodes, in principle a very highly anisotropic order parameter with a small uniform gap everywhere on the Fermi surface could mimic the behavior of a gap with nodes when inelastic scattering or experimental resolution smears the

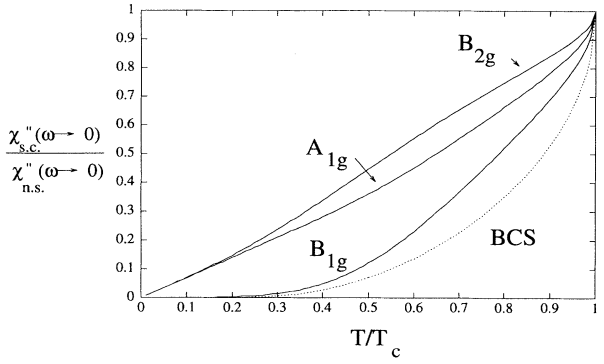

FIG. 2. Ratio of the low-frequency Raman response in the superconductor with $d_{x^2-y^2}$ pairing to the normal metal for the temperatures indicated. Note the slow decrease of the A_{1g} and B_{2g} channels with temperature.

threshold. In principle the detection of a threshold can then only be performed at very low temperatures where activated behavior can be observed. Since this remains a possibility, we now discuss two types of energy gaps which are anisotropic but have a finite gap around the Fermi surface.

C. Mixed-state pairing

Kotliar and Joynt have suggested the possibility that an order parameter which is a superposition of an s-wave and a d-wave gap can also provide an adequate description of the various transport and thermodynamic measurements on the cuprate systems.[41] The $s+id$ state has the interesting feature that in pure tetragonal superconductors there would be two transition temperatures associated with the formation of each gap separately. This is a consequence of the admixture of two different representations of the energy gap. However, orthorhombic distortions remove the $x \leftrightarrow y$ symmetry and thus A_{1g} and B_{1g} belong to the same representation. This leads then to one transition temperature. Since the orthorhombic distortions are quite small in the cuprates (judging from the observed phonons and selection rules), the transition temperature will be broad, which is in some conflict with the resistive transitions seen in the cuprates.

Nevertheless, we investigate what such a gap predicts for the Raman response by evaluating Eq. (33) in terms of leading-order Fermi-surface harmonics using a gap of the form $\Delta(\hat{\mathbf{k}}) = \Delta_s(T) + i\Delta_d(T)\cos(2\varphi)$. The results can written again in an analytic form in terms of complete elliptical integrals. Taking screening into account and defining $x^2 = [(\omega/2)^2 - \Delta_s^2]/\Delta_d^2$, we obtain, for $T = 0$,

$$\chi''^{\,sc}_{B_{1g}} = \chi''_{B_{1g}}(\mathbf{q}=0,\omega) = \Theta(x^2)\frac{4N_F\Delta_d\gamma^2_{B_{1g}}}{3\pi\omega}\begin{cases}[(2+x^2+3\Delta_s^2/\Delta_d^2)K(x)-(2+2x^2+3\Delta_s^2/\Delta_d^2)E(x)], & x\le 1,\\ x[(1+2x^2+3\Delta_s/\Delta_d^2)K(1/x)-(2+2x^2+3\Delta_s^2/\Delta_d^2)E(1/x)], & x>1,\end{cases} \tag{52}$$

$$\chi''^{\,sc}_{B_{2g}} = \chi''_{B_{2g}}(\mathbf{q}=0,\omega) = \Theta(x^2)\frac{4N_F\Delta_d\gamma^2_{B_{2g}}}{3\pi\omega}\begin{cases}[(1-x^2)K(x)-(1-2x^2-3\Delta_s^2/\Delta_d^2)E(x)], & x\le 1,\\ x\{[2-2x^2-3\Delta_s^2/\Delta_d^2(1-1/x^2)]K(1/x)\\ -(1-2/x^2-3\Delta_s^2/\Delta_d^2)E(1/x)\}, & x>1,\end{cases} \tag{53}$$

$$\chi^{sc}_{A_{1g}}(i\omega) = \chi_{A_{1g},A_{1g}}(i\omega) - \frac{\chi^2_{A_{1g},1}(i\omega)}{\chi_{1,1}(i\omega)}, \tag{54}$$

with the spectral functions

$$\chi''_{A_{1g},A_{1g}}(\mathbf{q}=0,\omega) = \Theta(x^2)\frac{4N_F\Delta_d\gamma^2_{A_{1g}}}{15\pi\omega}\begin{cases}\{[7-8x^2+16x^4-5\Delta_s^2/\Delta_d^2(1-4x^2)]K(x) \\ -[7-12x^2+32x^4-20\Delta_s^2/\Delta_d^2(1-2x^2)]E(x)\}, & x\le 1, \\ x\{[23-40x^2+32x^4+\frac{5\Delta_s^2}{\Delta_d^2x^2}(3-8x^2+8x^4)]K(1/x) \\ -[11-28x^2+32x^4-\frac{20\Delta_s^2}{\Delta_d^2x^2}(1-2x^2)]E(1/x)\}, & x>1,\end{cases} \tag{55}$$

$$\chi''_{A_{1g},1}(\mathbf{q}=0,\omega) = \Theta(x^2)\frac{2\sqrt{2}N_F\Delta_d\gamma_{A_{1g}}}{3\pi\omega}\begin{cases}[(1+2x^2+3\Delta_s^2/\Delta_d^2)K(x)-(1+4x^2+6\Delta_s^2/\Delta_d^2)E(x)], & x\le 1, \\ -x\{[1-4x^2+\frac{3\Delta_s^2}{\Delta_d^2x^2}(1-2x^2)]K(1/x) \\ +(1+4x^2+6\Delta_s^2/\Delta_d^2)E(1/x)\}, & x>1,\end{cases} \tag{56}$$

and

$$\chi''_{1,1}(\mathbf{q}=0,\omega) = \Theta(x^2)\frac{2N_F\Delta_d}{\pi\omega}\begin{cases}[(1+\Delta_s^2/\Delta_d^2)K(x)-E(x)], & x\le 1\ , \\ x[(1+\frac{\Delta_s^2}{\Delta_d^2x^2})K(1/x)-E(1/x)], & x>1.\end{cases} \tag{57}$$

The results are plotted in Fig. 3 using a value of $\Delta_s/\Delta_d = 0.25$. The finite gap Δ_s is responsible for the threshold appearing at $2\Delta_s$, which is the minimum energy required to break a Cooper pair. The spectra are polarization dependent, with the B_{2g} and A_{1g} spectra displaying a discontinuous jump at the threshold while the B_{1g} channel shows a continuous rise from zero to a peak at $\omega = 2\Delta_{\max} = 2\sqrt{\Delta_s^2+\Delta_d^2}$. Since both the A_{1g} and B_{2g} channels exhibit broad maxima for the case of a pure $d_{x^2-y^2}$ gap, the presence of the $2\Delta_s$ threshold will imply a shifting of the peak of the spectra away from the pure case to values lower in frequency if $2\Delta_s < \omega_{\text{peak}}$ (or at least create a shoulder at $2\Delta_s$), while also removing any difference in the peak position between the A_{1g} and B_{2g} channels. Taken by itself this cannot be reconciled with the experimental data unless of course Δ_s is very small.

We also note that similar behavior is expected for another time-reversal breaking state, namely, the $d_{x^2-y^2} + id_{xy}$ state as suggested by Rokhsar and Laughlin which arises from an anyon approach to the t-J model.[42] In terms of leading Fermi-surface harmonics, the state is represented as $\Delta(\phi) = \Delta_1\cos(2\phi) + i\Delta_2\sin(2\phi)$. The features of the Raman spectra are similar to those shown in Fig. 3, with $\Delta_2/\Delta_1 = 0.25$.

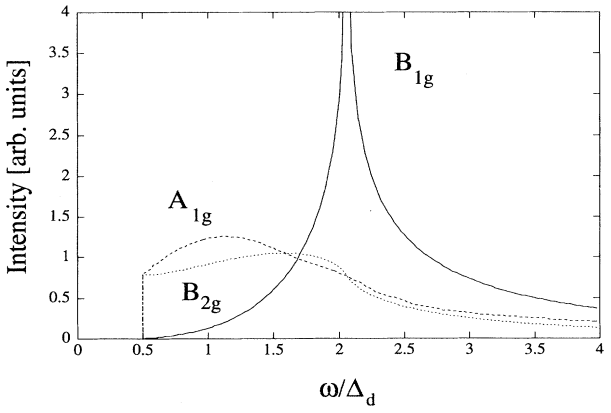

FIG. 3. Response functions for various symmetries for $s+id$ pairing with $\Delta_s/\Delta_d = 0.25$. All vertices are set to 1.

D. Anisotropic s-wave pairing

Combining the notion of interlayer Cooper pair tunneling as a mechanism for enhanced superconductivity in multilayer superconductors with simple band structure arguments, recently an anisotropic energy gap of the form

$$\Delta(\hat{\mathbf{k}}) = \Delta_0 + \Delta_1\cos^4(2\varphi) \tag{58}$$

has been proposed also to explain the cuprate materials.[43] This energy gap is anisotropic and shares the property of a $d_{x^2-y^2}$ energy gap in that it is largest for those directions where the $d_{x^2-y^2}$ gap has its largest absolute value. Yet the gap does not change sign around the Fermi surface. This is one specific example of an anisotropic s-wave energy gap, since the gap transforms in the same way as the band structure and thus has the same symmetry. While other representations for anisotropic s-wave gaps of course do exist [in particular, a possibility recently suggested by photoemission is $\Delta(\mathbf{k}) = \cos(k_xa) + \cos(k_ya) = \text{const} + A\cos(4\varphi)$ (Ref. 44)], we remark that the response calculated here is not qualitatively different from other cases and thus address only this one case.

Again we evaluate the Raman response for such a superconductor numerically and plot our results for $\Delta_0/\Delta_1 = 0.25$ in Fig. 4(a). Immediately we see similar behavior as in the previous case with one notable exception. While the spectra each show a $2\Delta_0$ threshold, the B_{2g} channel displays a BCS-like singularity at the threshold and the A_{1g} displays a large increase near the threshold that removes any trace of a peaklike structure in the spectra at higher frequencies. Again this would predict the same peak position (or a shoulder) for the A_{1g} and B_{2g} channels. Therefore, for Δ_0 not too small, it is not possible using just the symmetry of the gap alone to arrive at a situation where the peaks in the Raman spectra in the A_{1g} and B_{2g} channels lie at separate

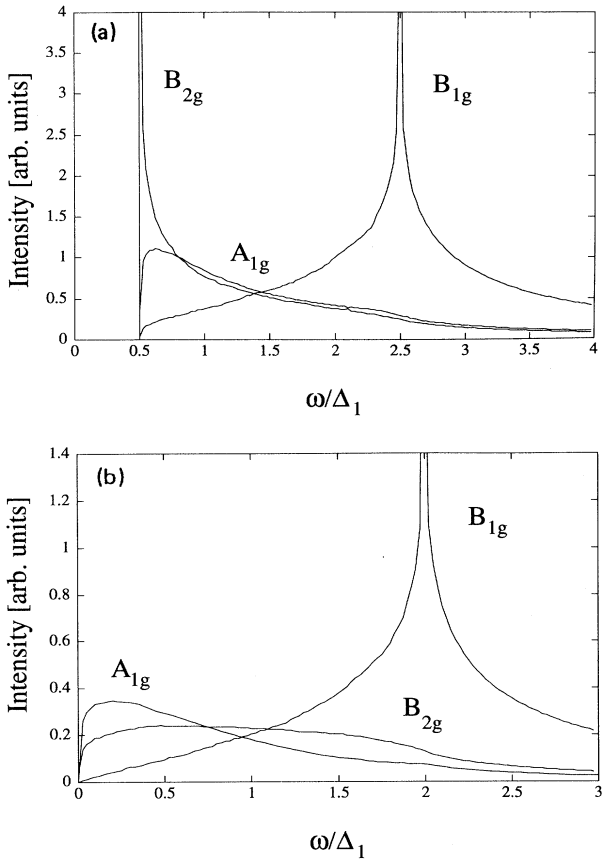

FIG. 4. Response functions for various symmetries for anisotropic s-wave pairing with (a) $\Delta_0/\Delta_1 = 0.25$ and (b) $\Delta_0 = 0$. All vertices are set to 1.

high energies, again which is not in agreement with experiments.

In principle the s-wave component of the gap can be made vanishingly small. We show the Raman spectra calculated for $\Delta_0 = 0$ in Fig. 4(b). The greater anisotropy of the energy gap compared to the $d_{x^2-y^2}$ case leads to a further anisotropy of the position of the peaks in each channel, with peaks in the spectra at $\omega = 2\Delta_{\max}$, $0.6\Delta_{\max}$, and $0.2\Delta_{\max}$ for the B_{1g}, B_{2g}, and A_{1g} channels, respectively, where $\Delta_{\max} = \Delta_0 + \Delta_1$. On top of this, the low-frequency power-law behavior is linear (with logarithmic corrections) in each channel, in contrast to the $d_{x^2-y^2}$ results. This is a general feature that the spectra become more and more polarization dependent the greater the anisotropy of the energy gap (compare to Fig. 1 for the $d_{x^2-y^2}$ case).

V. COMPARISON WITH DATA ON THE CUPRATE SYSTEMS AND CONCLUSIONS

In this section we present a comparison of the theory for a $d_{x^2-y^2}$ paired superconductor to recent measurements on the electronic Raman continuum in three cuprate superconductors. In what follows, we plot $S_{\gamma\gamma}(\omega)$, Eq. (1), which is given by χ of Eqs. (49)–(54) multiplied by the Bose factor. In drawing the fits to the spectra, the following procedure is employed. First the fit to the B_{1g} spectrum is made which determines the maximum value of the energy gap Δ_0 via the position of the peak in the spectrum. Next, the derived response is convoluted with a Gaussian which mimics the effect of a distribution of T_c values, inelastic scattering, finite z dispersion of the Fermi surface, experimental resolution, etc. Once this is done, the parameters remain fixed and only the prefactor of the vertex is left to be adjusted to match the overall intensity, which has no effect on the line shape. Since γ is in principle derivable from the band structure but presently is unknown even for such simple metals as aluminum, this remains a free parameter. It would be straightforward to include more accurate calculations for the magnitude of the vertex when they become available.

We first fit the data taken on single crystals of as-grown $Bi_2Sr_2CaCu_2O_8$ ($T_c = 90$ K) obtained in Ref. 19 for all symmetries at $T = 20$ K, where a subtraction procedure has been employed to ascertain the A_{1g} signal (see Sec. III A). The comparison of the theory with experiment is shown in Fig. 5. The parameters used to obtain the best fit to the spectrum are $\Delta_0 = 287$ cm^{-1} and a smearing width of $\Gamma/\Delta_0 = 0.15$. The theory gives good agreement with the data at low-frequency shifts while at higher-frequency shifts the theory fails to produce the broad continuum which is relatively constant up to the scale of 1 eV. This is most likely due to the neglect of impurities and/or electron-electron scattering,[45] which is beyond the scope of this paper. We see immediately that the peak positions in the B_{2g} and A_{1g} channels given by the theory automatically agree with the data. Also the asymptotic behavior of the continuum at low frequencies given by Eq. (51) is shown in the data when one neglects the phonons at roughly 100 and 330 wave numbers. Again, these power laws are intrinsic to a $d_{x^2-y^2}$ pair state. Last, the ratio of the intensity of the spectra in different channels is consistent with Eq. (35) and Fig. 2, which predicts that the B_{1g} channels shows the smallest intensity at low-frequencies while the A_{1g} channels shows the largest. All of the experimental features are

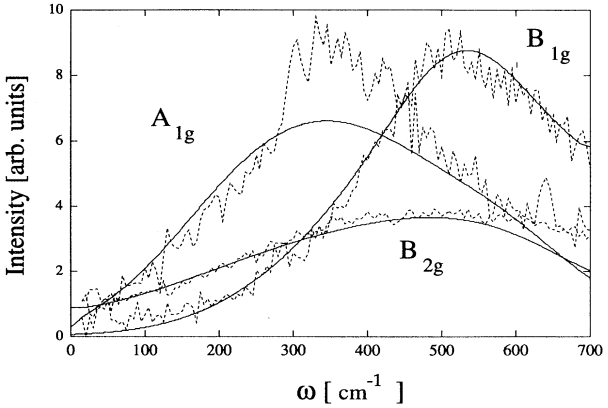

FIG. 5. Comparison of the theory to the experimental data taken on Bi-Sr-Ca-Cu-O from Ref. 19 using $d_{x^2-y^2}$ pairing. The parameters used are defined in the text.

thus consistent with the theory at least at low-frequency shifts $\omega < 1000$ cm^{-1}.

We now turn to the data taken on single crystals of $YBa_2Cu_3O_7$ ($T_c = 88$ K) obtained in Ref. 18 for all symmetries at $T = 20$ K, where the same subtraction procedure used in Bi-Sr-Ca-Cu-O was employed to ascertain the A_{1g} signal. The comparison of the theory to the data is shown in Fig. 6, with the parameters $\Delta_0 = 210$ cm^{-1} and $\Gamma/\Delta_0 = 0.2$ Again, the theory gives a good description of the data for $\omega < 1000$ cm^{-1}. We again see the peak positions at relatively the same place as in Bi-Sr-Ca-Cu-O and power laws linear in frequency at low shifts for the B_{2g} and A_{1g} channels. We note that while the cubic rise of the spectra predicted by the theory fits rather well with the B_{1g} data in Bi-Sr-Ca-Cu-O, we remark that the Fano effect of the B_{1g} phonon which appears to be stronger in Y-Ba-Cu-O than in Bi-Sr-Ca-Cu-O can obscure the rise of the spectra at low frequencies that give the appearance of a linear dependence on frequency.[46] Last, the ratios of the response in the static limit again are consistent with the theory.

Last, we investigate the single-layer thallium compound $Tl_2Ba_2CuO_6$ ($T_c = 80$ K) obtained in Ref. 20. The sample is most likely the most affected by disorder and therefore our theory will not be expected to give the best fit to the data. Our fits are shown in Fig. 7 for the B_{1g} and the mixed $A_{1g} + B_{2g}$ channels at $T = 20$ K. The value of the parameters used are $\Delta_0 = 232$ cm^{-1} and smearing width $\Gamma/\Delta_0 = 0.25$. All phonons have been subtracted. Once again the theory gives a good description of the relative peak positions. Considering also that this compound has only one Cu-O layer, the agreement of the theory with experiment also validates the assumption that the Raman scattering results predominantly from intraband fluctuations of the single Cu-O layer band and that interband scattering can be neglected. The theory also accounts for the linear rise of the spectrum for the A_{1g} channel for low frequencies. However, the theory cannot account for the linear rise of the spectrum in the B_{1g} channel. This most likely is due to the neglect of impurity scattering. The residual

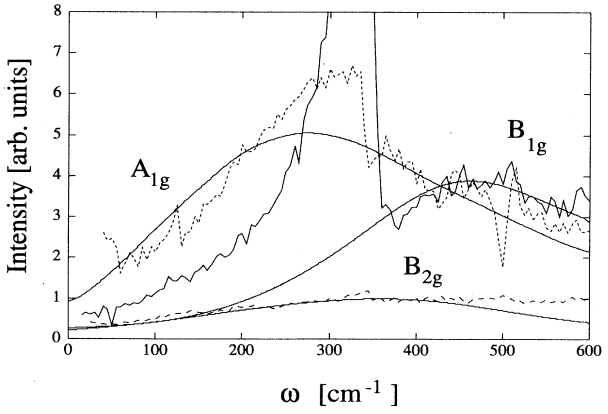

FIG. 6. Comparison of the theory to the experimental data taken on Y-Ba-Cu-O using $d_{x^2-y^2}$ pairing from Ref. 18. The parameters used are defined in the text.

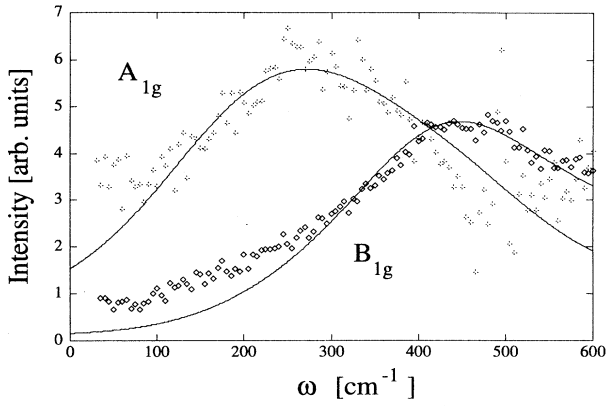

FIG. 7. Comparison of the theory to the experimental data taken on a single-layer thallium cuprate using $d_{x^2-y^2}$ pairing from Ref. 20. The parameters used are defined in the text.

scattering near zero-frequency shifts is also borne out by the theory, although the amount is underestimated for the B_{1g} channel. Again, this most likely has to do with the neglect of impurity scattering.

We remark that the theory is incomplete in that the theory fails to describe the flat continuum at large frequency shifts. Moreover, the theory cannot be extended to the normal state since the response functions vanish at T_c in the limit $q \to 0$ due to phase space restrictions. Here the additional physics of electron-electron scattering and/or impurity scattering must be incorporated to have a consistent theory to simultaneously describe the normal- and superconducting-state data. This is treated in detail in Ref. 31. Nevertheless, the low-frequency behavior of the spectra and, in particular, the relative peak positions of each polarization channel are quantitatively described by the theory.

In summary, we have seen that the Raman measurements on the cuprate systems provide a large body of symmetry-dependent information, all of which agrees with the predictions of $d_{x^2-y^2}$ pairing. Of course at present the information from Raman scattering alone cannot completely rule out the possibility of the presence of a very small gap which exists over the entire Fermi surface; nor can it determine whether the gap changes sign around the Fermi surface. For example, a gap of the form $\Delta \sim |\cos(2\varphi)|$ cannot be distinguished from a $d_{x^2-y^2}$ state [however, as shown in Sec. IV D, one can rule out a gap of the form $\Delta \sim \cos^{2n}(2\varphi)$, with $n > 1$]. Here it can be shown that the response of the spectra to impurity scattering can be of use.[31] However, the theoretical comparison shows that the gap must be predominantly of $|B_{1g}|$ character, and the low-temperature and low-frequency data seem to indicate that the minimum value of the gap must be very small if it exists at all. More precise measurements could of course clarify this point further. Also, more work is needed from band structures to pin down magnitude of the Raman tensor elements to predict the overall intensities.

ACKNOWLEDGMENTS

The authors would like to thank R. Hackl, G. Krug, R. Nemetschek, and B. Stadlober for providing us with their data and discussions. Similarly, we acknowledge enlightening discussions with J. C. Irwin, D. Reznik, R. R. P. Singh, R. T. Scalettar, A. Virosztek, A. Zawadowski, and G. T. Zimanyi, and thank A. Zawadowski for critically reading this manuscript. This work was supported in part by NSF Grant No. 92-06023 and by American Hungarian Joint Grant No. NSF 265/92b. One of the authors (T.P.D.) would like to acknowledge the hospitality of the Walther Meissner Institute, the Research Institute for Solid State Physics of the Hungarian Academy of Science, and the Institute of Physics of the Technical University of Budapest where parts of this work were completed.

APPENDIX A: RAMAN VERTICES AND FERMI SURFACE

In this appendix, we provide a connection between the Raman vertices and Fermi surface, and discuss the approximations made in Sec. IV in more detail. In order to proceed with the evaluation of Eq. (33), the Raman vertices must be evaluated on the Fermi surface. The 2D Fermi surface is defined through the relation $\epsilon(\mathbf{k}) = \mu$, where μ is the chemical potential, which in turn determines the Fermi momentum

$$\mathbf{k}_F = k_F(\varphi) \begin{pmatrix} \cos(\varphi) \\ \sin(\varphi) \end{pmatrix}. \tag{A1}$$

The scalar prefactor $k_F(\varphi)$ can be expanded with respect to the fully symmetric basis functions [A_{1g} or Γ_1^+ (Ref. 32)] for the tetragonal D^{4h} point group,

$$\begin{aligned} k_F(\varphi) &= k_F^{(0)} + k_F^{(2)} \cos(4\varphi) + k_F^{(4)} \cos(8\varphi) + \cdots \\ &= k_F^{(0)} + \sum_{L=1}^{\infty} k_F^{(2L)} \Phi_L^0(\varphi). \end{aligned} \tag{A2}$$

The higher-order Fourier coefficients $k_F^{(2L)}$ for $L > 0$ take into account deviations from cylindricity of the Fermi surface, $k_F^{(0)}$. The basis functions for the irreducible representations of the point group symmetry can be generalized as[35]

$$\Phi_L^{(\mu)}(\varphi) = \begin{cases} \cos[4L\varphi], & A_{1g}\ (\mu = 0), \\ \sin[(4L-2)\varphi], & B_{2g}\ (\mu = 1), \\ \sin[4L\varphi], & A_{2g}\ (\mu = 2), \\ \cos[(4L-2)\varphi], & B_{1g}\ (\mu = 3). \end{cases} \tag{A3}$$

Note that in case of a parabolic band dispersion the functions $\gamma_k^{(1)}$ and $\gamma_k^{(3)}$ vanish, whereas $\gamma_k^{(0)} = 2ma^2(t - 2t')$. This means that for a cylindrical Fermi surface only a constant A_{1g} component contributes to the Raman tensor. In other words, in order to have finite B_{1g} and B_{2g} Raman signals, the band structure must be expanded at least to fourth order and the Fermi surface can no longer be cylindrical in such a situation. We proceed now by expanding the functions $\gamma_k^{(\mu)}$, taken at the Fermi surface, in terms of Fermi-surface harmonics,

$$\begin{aligned} \gamma_k^{(\mu)}|_{\mathrm{FS}} = \gamma^{(\mu)}(\varphi) &= \sum_{L=1}^{\infty} \gamma_L^{(\mu)}\ \Phi_L^{(\mu)}(\varphi), \\ \gamma_L^{(\mu)} &= \int_0^{2\pi} \frac{d\varphi}{\pi} \Phi_L^{(\mu)}(\varphi)\gamma^{(\mu)}(\varphi). \end{aligned} \tag{A4}$$

It is important to note that the coefficients $\gamma_{L=1}^{(\mu)}$ corresponding to the lowest-order Fermi-surface harmonics $\Phi_{L=1}^{(\mu)}(\varphi)$ (except $\gamma_{L=1}^{(0)}$) *vanish* in the limit of parabolic band dispersion or cylindrical Fermi surface. They are finite only due to a deviation from cylindricity of the Fermi surface. Moreover, one may show that

$$\gamma_{L=1}^{(\mu)} = \gamma_{L=1}^{(\mu)}\{k_{F0}, k_{F1}, k_{F2}, k_{F3}, \ldots\}$$

is a functional of the full set of A_{1g} Fourier coefficients of the expansion of the Fermi wave number. It is therefore convenient to truncate the expansion into Fermi-surface harmonics after the lowest-order terms and treat the expansion coefficients as adaptable parameters. This completes the purpose of Appendix A.

APPENDIX B: WEAK-COUPLING RESULTS

In this appendix we show that gap anisotropy causes both the gap at zero temperature $\Delta_0(0)$ and the specific heat discontinuity at the transition $\Delta C/C_N$ (related to the slope of the gap function near T_c) to deviate from their respective BCS values of $[\Delta_0(0)/T_c]_{\mathrm{BCS}} = \pi \exp(-\gamma) = 1.7638...$ and $(\Delta C/C_N)_{\mathrm{BCS}} = 12/7\zeta(3) = 1.4261...$, with $\gamma = 0.577\,21...$ and $\zeta(3) = 1.202\,05...$ denoting Euler's constant and Riemann's ζ function, respectively. A straightforward solution of Eq. (18) leads to

$$\begin{aligned} \frac{\Delta_0(0)}{T_c} \equiv \delta_{\mathrm{sc}} &= \left(\frac{\Delta_0(0)}{T_c}\right)_{\mathrm{BCS}} \\ &\quad \times \exp\left(-\frac{\langle|\Delta_p|^2 \ln(|\Delta_p|/\Delta_0)\rangle_{\mathrm{FS}}}{\langle|\Delta_p|^2\rangle_{\mathrm{FS}}}\right), \\ \frac{\Delta C}{C_N} &= \left(\frac{\Delta C}{C_N}\right)_{\mathrm{BCS}} \frac{\langle|\Delta_p|^2\rangle_{\mathrm{FS}}^2}{\langle|\Delta_p|^4\rangle_{\mathrm{FS}}}. \end{aligned} \tag{B1}$$

These results may be used to generate an interpolation formula for the temperature dependence of the gap maximum $\Delta_0(T)$:

$$\Delta_0(T) = \delta_{\mathrm{sc}} T_c \tanh\left[\frac{\pi}{\delta_{\mathrm{sc}}}\sqrt{\frac{3}{2}\frac{\Delta C}{C_N}\frac{\Delta_0^2}{\langle|\Delta_p|^2\rangle_{\mathrm{FS}}}\left(\frac{T_c}{T} - 1\right)}\right]. \tag{B2}$$

For the special case of a gap with $d_{x^2-y^2}$ symmetry, one obtains, for δ_{sc} and $\Delta C/C_N$,

$$\begin{aligned} \delta_{\mathrm{sc}} &= 2\pi \exp\left(-\gamma - \frac{1}{2}\right) = 2.1397, \\ \Delta C/C_N &= \frac{12}{7\zeta(3)}\frac{2}{3} = 0.9507. \end{aligned} \tag{B3}$$

We should emphasize that these numbers should not be taken too seriously since they emerge from a weak-

coupling treatment. One should rather adopt the convention to treat them as parameters which can be adjusted to experiment and so account for strong-coupling effects in the trivial sense in which they appear as renormalizations of the quantities Δ_0 and $\Delta C/C_N$.

APPENDIX C: DIAGRAMMATIC GAUGE-INVARIANT RAMAN RESPONSE: ROLE OF VERTEX CORRECTIONS AND COLLECTIVE MODES

In this appendix we examine the role of final-state interactions and excitonic modes in unconventional superconductors. We use a diagrammatic approach which captures the effects of final-state interactions neglected in Sec. II. After solving the coupled integral equations for the renormalized vertex, we evaluate the position, broadening, and residue of the massive and massless collective modes as a function of coupling strength for a $d_{x^2-y^2}$ energy gap on a spherical Fermi surface. We then investigate the collective modes on a cylindrical (2D) Fermi surface by turning off any z dispersion in the band structure.

We begin by writing down the expression for the Raman two-particle response function in Nambu space as

$$\chi(\mathbf{q},i\omega) = -T\sum_{i\omega_n}\sum_{\mathbf{k}} \mathrm{Tr}\left[\hat{\Gamma}\left(\mathbf{k},\mathbf{q},i\omega\right)\hat{G}\left(\mathbf{k}+\frac{\mathbf{q}}{2},i\omega_n\right)\hat{\gamma}(\mathbf{k},-\mathbf{q})\hat{G}\left(\mathbf{k}-\frac{\mathbf{q}}{2},i\omega_n-i\omega\right)\right], \tag{C1}$$

$$\hat{\Gamma}(\mathbf{k},\mathbf{q},i\omega)-\hat{\gamma}(\mathbf{k},\mathbf{q}) = -T\sum_{i\omega_n}\sum_{\mathbf{p},\mathbf{p}'}\tau_3\hat{G}\left(\mathbf{p}+\frac{\mathbf{p}'}{2},i\omega_n\right)\hat{\Gamma}(\mathbf{p},\mathbf{p}',i\omega)\hat{G}\left(\mathbf{p}-\frac{\mathbf{p}'}{2},i\omega-i\omega_n\right) \times V\left(\mathbf{p}-\mathbf{k}+\frac{\mathbf{q}-\mathbf{p}'}{2},\mathbf{k}-\mathbf{p}+\frac{\mathbf{q}-\mathbf{p}'}{2}\right)\tau_3, \tag{C2}$$

where Tr denotes taking the trace, τ_i are Pauli matrices in Nambu space, and the Raman vertex $\hat{\gamma}=\tau_3\gamma(\mathbf{k})$. The dressed vertex $\hat{\Gamma}$ contains the interactions V responsible for maintaining gauge invariance.

If one replaces the dressed vertex Γ by the undressed one, Eq. (2), then of course Eq. (C1) is manifestly not gauge invariant, and in general the neglect of collective modes arising from a gauge-invariant treatment could in principle affect the overall spectrum. Usually the question of gauge invariance is rather an academic one since the modes that appear in BCS systems have little impact on the response functions of a superconductor. It is well known that due to the spontaneously broken U(1) gauge symmetry in s-wave superconductors, two collective modes appear: an optical one with a frequency of 2Δ which is damped and a soundlike mode, the Anderson-Bogoliubov mode, which is soft and lies in the gap for neutral superconductors but is raised to the plasmon energy by the long-range Coulomb forces via the Higgs mechanism. However, in unconventional superconductors, there can exist in principle additional Goldstone modes corresponding to the additional broken continuous symmetries such as SO_3^S spin rotational symmetry in spin-triplet systems plus SO_3^L orbital rotational symmetry in spin-singlet systems if the gap does not possess the full symmetry of the Fermi surface. In addition, massive collective modes and/or excitons can arise if the energy gap is degenerate or has an admixture of different representations from the point group. The massive modes can in principle lie below the gap edge and thus be relevant for the low-frequency dynamics of correlation functions. For example, the spectrum of collective modes in ^{3}He is well known in both phases and leads to observable effects.[25] However, the collective modes of possible d-wave states that might be candidates for strongly correlated systems are not as well understood.[47] There are indications that a d-wave state of $d_{x^2-y^2}$ is particularly favorable in systems with strong correlations,[48] thus underscoring the necessity of an understanding of the response functions and collective modes for such a superconductor.

We continue our calculation for the gauge-invariant Raman response by first expanding the renormalized matrix vertex $\hat{\Gamma}$ along the Fermi surface in terms of crystal harmonics,

$$\hat{\Gamma}(\hat{\mathbf{k}},i\omega) = \sum_{L,\mu}\hat{\Gamma}_L^{\mu}(i\omega)\phi_L^{\mu}(\hat{\mathbf{k}}), \tag{C3}$$

and do the same for the pairing interaction,

$$V(\hat{\mathbf{k}},\hat{\mathbf{p}}) = \sum_{L,L';\mu,\mu'} V_{L,L'}^{\mu,\mu'}\phi_L^{\mu}(\hat{\mathbf{k}})\phi_{L'}^{\mu'}(\hat{\mathbf{p}}). \tag{C4}$$

The integral equation for the renormalized vertex at $\mathbf{q}=0$ can then be written as

$$\hat{\Gamma}_L^{\mu}(i\omega)-\hat{\gamma}_L^{\mu} = -\frac{TN_F}{2}\sum_{i\omega_n}\int d\epsilon d\epsilon' \sum_{L',L'';\mu',\mu''} V_{L,L'}^{\mu,\mu'}\langle\phi_{L''}^{\mu''}(\hat{\mathbf{k}})\phi_{L'}^{\mu'}(\hat{\mathbf{k}})\tau_3\hat{G}(\hat{\mathbf{k}},i\omega_n-i\omega)\hat{\Gamma}_{L''}^{\mu''}(i\omega)\hat{G}(\hat{\mathbf{k}},i\omega_n)\tau_3\rangle. \tag{C5}$$

Equation (C5) is completely general for any type of vertex, interaction, and gap symmetry. In particular, for the case of an isotropic energy gap, Eq. (C5) recovers the previously obtained results.[8,9] We confine ourselves to the case of singlet energy gaps and use the BCS approximation

$$\hat{G}(\mathbf{k}, i\omega_n) = \frac{i\omega_n + \xi\tau_3 + \Delta(\hat{\mathbf{k}})\tau_1}{(i\omega_n)^2 - E^2(\mathbf{k})}. \tag{C6}$$

More complicated Green's functions could be treated with the same scheme. However, the analysis gets considerably more complicated and cannot be carried as far analytically.

In general the pairing interaction V can have off-diagonal as well as diagonal terms in the L basis, and in general all channels will be coupled. If the interaction has the symmetry of the Fermi surface, then the integral equations only couple different channels L and L' which transform according to the same irreducible representation. However, the subsequent matrix can be diagonalized with respect to the indices of the same representation, resulting in a new set of basis functions which are linear combinations of the old basis functions of the same representation in different L channels.[49] Thus we can then write the interaction as a diagonal matrix in the new basis functions which still has a general structure for each representation within each new channel. Thus we can write $V^{\mu,\mu'}_{L,L'} = V^{\mu}_{L}\delta_{L,L'}\delta_{\mu,\mu'}$. This allows us to reduce the infinite series of coupled integral equations to a limited subset that can be handled analytically. The elements of the expansion will be dominated by a single V^{μ}_{L} component corresponding to the L pairing channel symmetry μ, and the other components represent admixtures of channels (the smaller eigenvalues in the gap equation) with different pairing symmetry. If the gap representation is one dimensional (all representations of the D^{4h} group except E_g, which is two dimensional), then all the other V^{μ}_{L}'s are set to zero and there will only be collective modes connected with the broken U(1) gauge invariance. Otherwise other collective modes can be present as well.

We now define new vertices $\hat{\Gamma}^{\mu}_{L}(i\omega) = \hat{\gamma}^{\mu}_{L} + V^{\mu}_{L}\hat{\delta}^{\mu}_{L}(i\omega)$ and expand $\hat{\delta}^{\mu}_{L}(i\omega)$ in spin quarternions,

$$\hat{\delta}^{\mu}_{L}(i\omega) = \sum_{i=0}^{3} \delta^{(i)\mu}_{L}(i\omega)\tau_i. \tag{C7}$$

The index μ stands for the representations of the D^{4h} point group, and are defined through the basis functions as

$$\phi^{\mu}_{L=2}(\hat{\mathbf{k}}) = \begin{cases} \frac{1}{\sqrt{2}}(k_x^2 - k_y^2), & B_{1g}(\Gamma_3^+)\ (\mu = 1), \\ \frac{1}{\sqrt{6}}(2k_z^2 - k_x^2 - k_y^2), & A_{1g}(\Gamma_1^+)\ (\mu = 2), \\ k_x k_y, & B_{2g}(\Gamma_4^+)\ (\mu = 3), \\ k_x k_z, & E_g(\Gamma_5^+)\ (\mu = 4), \\ k_y k_z, & E_g(\Gamma_5^+)\ (\mu = 5), \end{cases} \tag{C8}$$

where the Γ_i^+ corresponds to the notation of Sigrist and Rice.[32] It can be shown that the coefficients $\delta^{(0,1)\mu}_{L}$ of the Pauli matrices $\tau_{0,1}$ satisfy homogeneous equations and thus vanish while the remaining coefficients satisfy the coupled integral equations

$$\delta^{(2)\mu}_{L}(i\omega) = \sum_{L';\mu'} \left\{ V^{\mu}_{L'}\delta^{(2)\mu}_{L'}(i\omega) C^{-,\mu,\mu'}_{L,L'}(i\omega) + i[\gamma^{\mu'}_{L'} + V^{\mu'}_{L'}\delta^{(3)\mu'}_{L'}(i\omega)] A^{\mu,\mu'}_{L,L'}(i\omega) \right\}, \tag{C9}$$

$$\delta^{(3)\mu}_{L}(i\omega) = \sum_{L';\mu'} \left\{ iV^{\mu'}_{L'}\delta^{(2)\mu'}_{L'}(i\omega) A^{\mu,\mu'}_{L,L'}(i\omega) - [\gamma^{\mu}_{L'} + V^{\mu}_{L'}\delta^{(3)\mu}_{L'}(i\omega)] C^{+,\mu,\mu'}_{L,L'}(i\omega) \right\}, \tag{C10}$$

where the functions $A, C^{\pm}$ are given by

$$A^{\mu,\mu'}_{L,L'}(i\omega) = \langle \phi^{\mu}_{L}(\hat{\mathbf{k}})\phi^{\mu'}_{L'}(\hat{\mathbf{k}}) A(\hat{\mathbf{k}}, i\omega) \rangle,$$
$$C^{\pm\mu,\mu'}_{L,L'}(i\omega) = \langle \phi^{\mu}_{L}(\hat{\mathbf{k}})\phi^{\mu'}_{L'}(\hat{\mathbf{k}}) C^{\pm}(\hat{\mathbf{k}}, i\omega) \rangle. \tag{C11}$$

The spectral functions are defined as

$$A(\hat{\mathbf{k}}, i\omega) = -i\Delta(\hat{\mathbf{k}})\omega N_F \int d\xi \frac{1}{4E^2} \frac{1 - 2f(E)}{i\omega - 2E} - (i\omega \to -i\omega),$$
$$C^{+}(\hat{\mathbf{k}}, i\omega) = -N_F \int d\xi \frac{\Delta(\hat{\mathbf{k}})^2}{2E^2} \frac{1 - 2f(E)}{i\omega - 2E} + (i\omega \to -i\omega),$$
$$C^{-}(\hat{\mathbf{k}}, i\omega) = -\frac{N_F}{2} \int d\xi \frac{1 - 2f(E)}{i\omega - 2E} + (i\omega \to -i\omega). \tag{C12}$$

Here f is a Fermi function and $(i\omega \to -i\omega)$ denotes additional terms which differ only in the sign of $i\omega$. Analytically continuing to the real axis by letting $i\omega \to \omega + i0$, the ξ integration can be performed analytically and we obtain

$$
\begin{aligned}
A(\hat{\mathbf{k}},\omega) &= \Delta(\hat{\mathbf{k}})\ \ F(\hat{\mathbf{k}},\omega), \\
C^{+}(\hat{\mathbf{k}},\omega) &= \frac{2\Delta^2(\hat{\mathbf{k}})}{\omega} F(\hat{\mathbf{k}},\omega), \\
C^{-}(\hat{\mathbf{k}},\omega) &= \frac{1}{V(\hat{\mathbf{k}})} + \frac{\omega}{2} F(\hat{\mathbf{k}},\omega),
\end{aligned}
\tag{C13}
$$

with

$$
F(\hat{\mathbf{k}},\omega) = \begin{cases} \frac{N_F}{\sqrt{\Delta(\hat{\mathbf{k}})^2-(\omega/2)^2}} \arctan\left[\frac{\omega}{2\sqrt{\Delta(\hat{\mathbf{k}})^2-(\omega/2)^2}}\right] & \text{for } \Delta(\hat{\mathbf{k}})^2 > (\frac{\omega}{2})^2, \\ \frac{N_F}{2\sqrt{(\omega/2)^2-\Delta(\hat{\mathbf{k}})^2}} \left(i\pi + \ln\left[\frac{\omega/2-\sqrt{(\omega/2)^2-\Delta(\hat{\mathbf{k}})^2}}{\omega/2+\sqrt{(\omega/2)^2-\Delta(\hat{\mathbf{k}})^2}}\right]\right) & \text{for } \Delta(\hat{\mathbf{k}})^2 \le (\frac{\omega}{2})^2, \end{cases}
\tag{C14}
$$

and

$$
\frac{1}{V(\hat{\mathbf{k}})} = N_F \int_0^{\infty} \frac{d\xi}{2E(\mathbf{k})}
\tag{C15}
$$

given by the BCS gap equation. The function F is closely related to the Tsuneto function, Eq. (11).

The integral equations are still general for a charge-density-like vertex and the symmetries of the interaction and gap remain undefined. We now restrict our attention to the case of d-wave interactions such that only $V^{\mu}_{L=2} \neq 0$ and other terms corresponding to interactions in higher-angular-momentum channels are discarded. Dropping the $L=2$ subscript by denoting $V^{\mu}_{L=2}$ by V_{μ} and $\delta^{(2,3)\mu}_{L=2}$ by $\delta^{(2,3)}_{\mu}$, the integral equations simplify to

$$
\delta^{(2)}_{\mu}(i\omega) = \sum_{\mu'} \left\{ V_{\mu'} [\delta^{(2)}_{\mu'}(i\omega) C^{-\mu,\mu'}_{L=2,L=2}(i\omega) + i\delta^{(3)}_{\mu'}(i\omega) A^{\mu,\mu'}_{L=2,L=2}(i\omega)] + i \sum_{L'} \gamma^{\mu'}_{L'} A^{\mu,\mu'}_{L=2,L'}(i\omega) \right\},
\tag{C16}
$$

$$
\delta^{(3)}_{\mu}(i\omega) = \sum_{\mu'} \left\{ V_{\mu'} [-\delta^{(3)}_{\mu'}(i\omega) C^{+\mu,\mu'}_{L=2,L=2}(i\omega) + i\delta^{(2)}_{\mu'}(i\omega) A^{\mu,\mu'}_{L=2,L=2}(i\omega)] - \sum_{L'} \gamma^{\mu}_{L'} C^{+\mu,\mu'}_{L=2,L'}(i\omega) \right\}.
\tag{C17}
$$

These equations are still general to any d-wave pair state.

We now specifically work with a $d_{x^2-y^2}$ gap $\Delta(\hat{\mathbf{k}}) = \Delta_0(\hat{k}_x^2 - \hat{k}_y^2)$ (the Γ_3^+ representation[32]), noting that a similar conclusion can be drawn for other choices of energy gaps within the $L=2$ subgroup of the D^{4h} point group. We allow for generalized interactions in the $L=2$ channel, which allows for the presence of excitons. The coupled integral equations represent ten equations for the ten unknowns $\delta^{(i)}_{\mu}, i \in \{2,3\}$, and the solution can be obtained by diagonalizing a 10×10 matrix.

We first simplify our notation by defining

$$
\begin{aligned}
f^{A}_{\mu}(i\omega) &= \sum_{L,\mu'} \gamma^{\mu'}_{L} A^{\mu,\mu'}_{L=2,L}(i\omega), \\
f^{C}_{\mu}(i\omega) &= -\sum_{L,\mu'} \gamma^{\mu'}_{L} C^{+\mu,\mu'}_{L=2,L}(i\omega).
\end{aligned}
\tag{C18}
$$

We find that the $\mu = 1(B_{1g})$ and $\mu = 2(A_{1g})$ channels are coupled due to the fact that a $d_{x^2-y^2}$ energy gap squared has a component which has a finite overlap with the A_{1g} channel which is isotropic within the x-y plane. Solving the integral equations we obtain, for the $\mu = 1$ (B_{1g}) and $\mu = 2$ (A_{1g}) channels,

$$
\begin{aligned}
\delta^{(2)}_{1}(i\omega) &= i \frac{f^{A}_{1}(i\omega) + V_2 A^{1,2}_{2,2}(i\omega)\delta^{(3)}_{2}(i\omega)}{1 - V_1 C^{-1,1}_{2,2}(i\omega)}, \\
\delta^{(3)}_{1}(i\omega) &= \frac{f^{C}_{1}(i\omega) - V_2 \frac{f^{A}_{2}(i\omega) A^{1,2}_{2,2}(i\omega)}{1 - V_2 C^{-2,2}_{2,2}(i\omega)}}{1 + V_1 C^{+1,1}_{2,2}(i\omega) + \frac{V_1 V_2 |A^{1,2}_{2,2}(i\omega)|^2}{1 - V_2 C^{-2,2}_{2,2}(i\omega)}}, \\
\delta^{(2)}_{2}(i\omega) &= i \frac{f^{A}_{2}(i\omega) + V_1 A^{1,2}_{2,2}(i\omega)\delta^{(3)}_{1}(i\omega)}{1 - V_2 C^{-2,2}_{2,2}(i\omega)}, \\
\delta^{(3)}_{2}(i\omega) &= \frac{f^{C}_{2}(i\omega) - V_1 \frac{f^{A}_{1}(i\omega) A^{1,2}_{2,2}(i\omega)}{1 - V_1 C^{-1,1}_{2,2}(i\omega)}}{1 + V_2 C^{+2,2}_{2,2}(i\omega) + \frac{V_1 V_2 |A^{1,2}_{2,2}(i\omega)|^2}{1 - V_1 C^{-1,1}_{2,2}(i\omega)}}.
\end{aligned}
\tag{C19}
$$

For the $\mu = 3(B_{2g})$ and $\mu = 4,5$ (two E_g) channels, we find no coupling and obtain

$$
\begin{aligned}
\delta^{(2)}_{3}(i\omega) &= i \frac{f^{A}_{3}(i\omega)}{1 - V_3 C^{-3,3}_{2,2}(i\omega)}, \\
\delta^{(3)}_{3}(i\omega) &= \frac{f^{C}_{3}(i\omega)}{1 + V_3 C^{+3,3}_{2,2}(i\omega)},
\end{aligned}
\tag{C20}
$$

$$\delta^{(2)}_{4,5}(i\omega) = i\frac{f^{A}_{4,5}(i\omega) + V_{4,5}A^{4,4;5,5}_{2,2}(i\omega)\delta^{(3)}_{4,5}(i\omega)}{1 - V_{4,5}C^{-4,4;5,5}_{2,2}(i\omega)},$$

$$\delta^{(3)}_{4,5}(i\omega) = \frac{f^{C}_{4,5}(i\omega) - V_{4,5}\frac{f^{A}_{4,5}(i\omega)A^{4,4;5,5}_{2,2}(i\omega)}{1-V_{4,5}C^{-4,4;5,5}_{2,2}(i\omega)}}{1 + V_{4,5}C^{+4,4;5,5}_{2,2}(i\omega) + \frac{|V_{4,5}A^{4,4;5,5}_{2,2}(i\omega)|^2}{1-V_{4,5}C^{-4,4;5,5}_{2,2}(i\omega)}}, \tag{C21}$$

where $V_{4,5}$, $\delta_{4,5}$, $C^{\pm 4,4;5,5}$, and $A^{4,4;5,5}$ stand for the interactions, renormalized vertices, and spectral functions in the $\mu = 4, 5$ channels, respectively. These equations represent the full channel-dependent renormalization of the Raman vertex due to general d-wave pairing interactions.

We now are in a position to identify the collective modes in the ten channels (five real and five imaginary). The modes are of two types, namely, massive and massless. The massless (Goldstone) modes are a consequence of the spontaneously broken continuous symmetries, while the massive (optical or excitonic) modes are generated by the presence of interactions in several channels. Using Eqs. (C19)–(C21), in each channel we locate the zeros of the real part of the denominator in each channel to find the position of the collective mode and evaluate the imaginary part of the denominator at the position of the collective mode to determine its broadening.

Our results are summarized in Table I for various strengths of the interactions in each channel. We see that the Goldstone mode ($\omega_c = 0$), which arises due to U(1) symmetry breaking, appears in the A_{1g} channel while the other modes are massive (excitonic). The B_{1g} modes lie beneath the maximum energy gap while the others appear above $2\Delta_0$. It was shown by Monien and Zawadowski[9] that depending on the sign of the residual interaction, excitonic or electron pair bound states can be formed. These excitonic or electron pair modes are damped considerably due to the existence of quasiparticles from the presence of gap nodes which provide decay channels to damp the massive modes. This is in contrast to excitonic modes in s-wave superconductors.[9,10] However, we do observe in Table I that the mode position rapidly decreases to lower frequencies with depreciating residue as the coupling strength $V_\mu/V_{B_{1g}}$ is reduced, which is similar to the BCS case. Below a critical coupling strength $V_\mu/V_{B_{1g}} \sim 0.8$ the collective modes disappear altogether and thus have little impact on the low-frequency behavior of the Raman correlation function for small couplings.

We now reconstruct the Raman response and determine which of the collective modes couple to the Raman vertex. Putting in Eqs. (C19)–(C21) into (C1), we can express the full gauge-invariant Raman response function as

$$\chi^{\mu}_{L}(\mathbf{q}=0, i\omega) = 2\gamma^{\mu}_{L}\sum_{\mu'}\left(\sum_{L'}\gamma^{\mu'}_{L'}C^{+\mu,\mu'}_{L,L'}(i\omega) + V_{\mu'}\delta^{(3)}_{\mu'}(i\omega)C^{+\mu,\mu'}_{L,2}(i\omega) - iV_{\mu'}\delta^{(2)}_{\mu'}(i\omega)A^{\mu,\mu'}_{L,2}(i\omega)\right). \tag{C22}$$

Taking only the $L = 0, 2$ terms of the Raman vertex into account (see Sec. III), we carry out the summation over L' and μ' to obtain the Raman spectrum in each channel, and then take into account the long-range Coulomb screening via Eq. (32).

We find that for the $L = 0$ or density channel, $\chi(\mathbf{q} = 0, \omega) = 0$, which is a restatement of particle number conservation and bears out the gauge-invariant nature of the theory. This simply restates that intercell charge fluctuations couple to the long-range Coulomb forces to be completely screened for $q \to 0$. After lengthy but trivial algebra we obtain compact results for the intracell fluctuation contributions. For the B_{1g} channel we obtain

TABLE I. Position $\omega_c/2\Delta_0$ and broadening $\Gamma_c/2\Delta_0$ of the pole in $\delta^{(2,3)}_m$ for each channel for the interaction strength given. A Goldstone mode is present in the A_{1g} channel. Here, $V_1 N_F = 0.25$ has been used.

B_{1g}	$\delta^{(2)}_1$		$\delta^{(3)}_1$		B_{2g}	$\delta^{(2)}_3$		E_g	$\delta^{(2)}_{4,5}$		$\delta^{(3)}_{4,5}$	
$\frac{V_2}{V_1}$	$\frac{\omega_c}{2\Delta_0}$	$\frac{\Gamma_c}{2\Delta_0}$	$\frac{\omega_c}{2\Delta_0}$	$\frac{\Gamma_c}{2\Delta_0}$	$\frac{V_3}{V_1}$	$\frac{\omega_c}{2\Delta_0}$	$\frac{\Gamma_c}{2\Delta_0}$	$\frac{V_{4,5}}{V_1}$	$\frac{\omega_c}{2\Delta_0}$	$\frac{\Gamma_c}{2\Delta_0}$	$\frac{\omega_c}{2\Delta_0}$	$\frac{\Gamma_c}{2\Delta_0}$
1.0	0.89	0.17	0.83	0.20	1.0	1.16	0.23	1.0	1.16	0.23	1.09	0.22
0.98	0.73	0.16	0.70	0.19	0.98	1.04	0.21	0.98	1.05	0.21	0.98	0.21
0.96	0.60	0.15	0.59	0.18	0.96	0.90	0.19	0.96	0.93	0.19	0.87	0.19
0.94	0.49	0.14	0.48	0.16	0.94	0.78	0.17	0.94	0.78	0.16	0.74	0.16
0.92	0.39	0.13	0.39	0.15	0.92	0.59	0.13	0.92	0.62	0.13	0.55	0.13
0.90	0.30	0.11	0.30	0.13	0.90	0.37	0.08	0.90	0.36	0.08	0.32	0.08
0.88	0.22	0.09	0.22	0.11	0.88	no pole		0.88	no pole		no pole	
0.86	0.13	0.07	0.13	0.08	0.86	no pole		0.86	no pole		no pole	
0.84	0.05	0.04	0.05	0.04	0.84	no pole		0.84	no pole		no pole	
0.82	no pole		no pole		0.82	no pole		0.82	no pole		no pole	

$$\chi_{B_{1g}}(i\omega) = 2(\gamma_2^1)^2 \frac{C_{B_{1g}}(i\omega)}{1 + V_1 C_{B_{1g}}(i\omega)}, \tag{C23}$$

for the B_{2g} channel,

$$\chi_{B_{2g}}(i\omega) = 2(\gamma_2^3)^2 \frac{C_{B_{2g}}(i\omega)}{1 + V_3 C_{B_{2g}}(i\omega)}, \tag{C24}$$

and for the two E_g channels,

$$\chi_{E_g}(i\omega) = 2(\gamma_2^{4,5})^2 \frac{C_{E_g}(i\omega)}{1 + V_{4,5} C_{E_g}(i\omega)}, \tag{C25}$$

with the functions

$$C_{B_{1g}}(i\omega) = C_{2,2}^{+1,1}(i\omega) + V_2 \frac{|\, A_{2,2}^{1,2}(i\omega)\,|^2}{1 - V_2 C_{2,2}^{-2,2}(i\omega)}, \tag{C26}$$

$$C_{B_{2g}}(i\omega) = C_{2,2}^{+3,3}(i\omega), \tag{C27}$$

$$C_{E_g}(i\omega) = C_{2,2}^{+4(5),4(5)}(i\omega) + V_{4(5)} \frac{|\, A_{2,2}^{4(5),4(5)}(i\omega)\,|^2}{1 - V_{4(5)} C_{2,2}^{-4(5),4(5)}(i\omega)}. \tag{C28}$$

These channels are unaffected by screening since the intracell fluctuations lead to no net charge transfer for these symmetries. The expression for the fully symmetric A_{1g} channel which contains both intercell and intracell fluctuations expression is much more complicated due to Coulomb screening,

$$\chi_{A_{1g}}(i\omega) = 2\gamma_2^2 [C_{2,2}^{+2,2}(i\omega) - C_{2,0}^{+2,0}(i\omega)^2 / C_{0,0}^{+0,0}(i\omega)] \times \frac{1 - \frac{\gamma_0}{\gamma_2} V_2 C_{A_{1g}}^0(i\omega)}{1 + V_2 C_{A_{1g}}(i\omega)}. \tag{C29}$$

Here the functions $C_{A_{1g}}, C_{A_{1g}}^0$ are defined as

$$C_{A_{1g}}(i\omega) = C_{2,2}^{+2,2}(i\omega) + V_1 \frac{|\, A_{2,2}^{1,2}(i\omega)\,|^2}{1 - V_1 C_{2,2}^{-1,1}(i\omega)} \tag{C30}$$

and

$$C_{A_{1g}}^0(i\omega) = C_{2,0}^{+2,0}(i\omega) + V_1 \frac{A_{2,2}^{1,2}(i\omega) A_{2,0}^{1,0}(i\omega)}{1 - V_1 C_{2,2}^{-1,1}(i\omega)}. \tag{C31}$$

Examining the structure of the denominator of Eqs. (C23)–(C31), we see that the massless gauge mode (Goldstone mode) in the A_{1g} channel drops out of the Raman response, and only provides transverse screening via Eq. (32). The massive modes do appear in the B_{1g} and E_g channels while the massive mode found in the B_{2g} channel does not couple to a Raman probe. Linearizing the denominator around the position of the collective mode we calculate the residue Z of the mode to be $Z_{B_{1g}} = \omega_c / \ln(\Delta_0/\omega_c)$ and $Z_{E_g} = \omega_c$, where ω_c is the position of the collective mode in each channel.

Therefore, putting all our results together for the collective modes, we can argue that the collective modes are of little relevance to electronic Raman scattering due to the fact that (1) the modes only exist at beyond a large strong-couplings threshold, (2) the residue of the modes decreases the lower the position of the collective mode, and (3) the broadening of the collective modes is substantial.

However, of course, the final-state interactions themselves can affect the spectrum.[9,10] Therefore we display our results in Figs. 8(a)–8(c) for the entire spectrum in

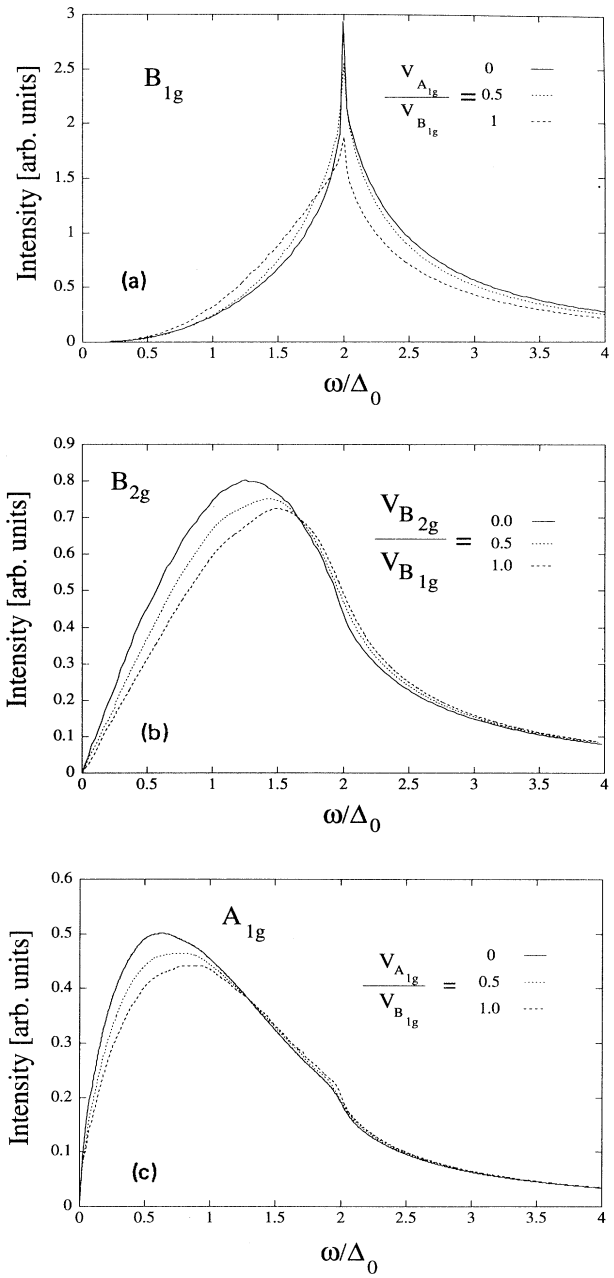

FIG. 8. Effect of vertex corrections on the Raman response evaluated for $d_{x^2-y^2}$ pairing on a spherical Fermi surface for (a) B_{1g}, (b) B_{2g}, and (c) A_{1g} channels (using $\gamma_0/\gamma_2 = 2$, other vertices set equal to 1). The E_g results look identical to the B_{2g} spectra. Here we have used $V_{B_{1g}} N_F = 0.2$, and the values of $V_m/V_{B_{1g}}$ are indicated in the upper right-hand corner of the figure.

the B_{1g}, B_{2g}, and A_{1g} channels for different ratios of the parameter $V_\mu/V_{B_{1g}}$, where $V_{B_{1g}}$ is the pairing interaction of $d_{x^2-y^2}$ symmetry. The response for the E_g channels is similar to the B_{2g} case. We note that the interactions have only a minor affect on the spectra in the B_{1g} channel, only changing the cusp behavior near $2\Delta_0$ while leaving the peak position and low-frequency behavior unchanged. The interactions have more an effect in the B_{2g} and A_{1g} channels due to the fact that the peaks of the spectra are very broad. Therefore the interactions shift the peak position upwards in frequency along the top of the broad hump of the spectrum, from $1.3\Delta_0$ to $1.5\Delta_0$ for the B_{2g} channel, and from $0.6\Delta_0$ to $0.8\Delta_0$ in the A_{1g} channel. Again we note that the low-frequency behavior remains unchanged. A similar effect is seen in the E_g channels. In particular, the massive mode in this channel is entirely damped, leading to no drastic changes in the spectrum.

We close this appendix by addressing the collective modes for a superconductor with a cylindrical (2D) Fermi surface. In a 2D system the only interactions that appear at the $L = 2$ level are the B_{1g} and B_{2g} channels, while the A_{1g} and A_{2g} channels appear at $L = 4$. Similarly, there are no E_g channels for a system without dispersion in the z direction. Therefore, if we are only concerned with d-wave interactions and not those of higher-angular-momentum channels, then we can set the matrix elements $V_{A_{1g}} = V_{E_g(1,2)} = 0$ in Eqs. (C19)–(C21) and the equations simplify greatly. Since then there will be no channel mixing of the A_{1g} channels into the response, therefore there can be no collective mode since no term appears in the denominators which has the form $1 - V_\mu/V_{B_{1g}}$ which arises through the function C^- [see Eqs. (C19)–(C21)]. Therefore we can conclude that collective modes can only appear when the interactions are included in higher-order L channels for a 2D system. Furthermore, the vertex corrections produce minor changes in the spectra only for the B_{1g} and B_{2g} channels. The changes are similar to the changes shown for the response functions evaluated on a spherical Fermi surface (apart from cutting off the logarithmic divergence of the B_{1g} response at the gap edge), and thus are not of major importance. We can therefore neglect the collective modes entirely and the effect of vertex corrections and simply use the pair approximation for the Raman response. This completes the purpose of this appendix.

[1] See, e.g., M. Sigrist and K. Ueda, Rev. Mod. Phys. **63**, 239 (1991); D. Pines, Physica **199-200**, 300 (1994); D. J. Scalapino, Phys. Rep. **250**, 329 (1995).

[2] Z.-X. Shen *et al.*, Phys. Rev. Lett. **70**, 1553 (1993); Z.-X. Shen, J. Phys. Chem. Solids **53**, 1583 (1992).

[3] D. A. Wollman *et al.*, Phys. Rev. Lett. **71**, 2134 (1993); A. G. Sun *et al.*, *ibid.* **72**, 2267 (1994); P. Chaudhari and S.-Y. Lin, *ibid.* **72**, 1048 (1994); C. C. Tsuei *et al.*, *ibid.* **73**, 593 (1994); A. Mathai *et al.* (unpublished).

[4] J. A. Martindale *et al.*, Phys. Rev. Lett. **68**, 702 (1992); P. C. Hammel, M. Takigawa, R. H. Heffner, Z. Fisk, and K. C. Ott, *ibid.* **63**, 1992 (1989); W. N. Hardy, D. A. Bonn, D. C. Morgan, R. Liang, and K. Zhang, *ibid.* **70**, 3999 (1993); Z. Ma *et al.*, *ibid.* **71**, 781 (1993); S. Anlage *et al.*, Phys. Rev. B **44**, 9764 (1991).

[5] J. Kosztin and A. Zawadowski, Solid State Commun. **78**, 1029 (1991).

[6] A. A. Abrikosov and L. A. Fal'kovskii, Zh. Eksp. Teor. Fiz. **40**, 262 (1961) [Sov. Phys. JETP **13**, 179 (1961)].

[7] A. A. Abrikosov and V. M. Genkin, Zh. Eksp. Teor. Fiz. **65**, 842 (1973) [Sov. Phys. JETP **38**, 417 (1974)].

[8] M. V. Klein and S. B. Dierker, Phys. Rev. B **29**, 4976 (1984).

[9] H. Monien and A. Zawadowski, Phys. Rev. B **41**, 8798 (1990).

[10] T. P. Devereaux, Phys. Rev. B **45**, 12 965 (1992); **47**, 5230 (1993).

[11] T. P. Devereaux, D. Einzel, B. Stadlober, R. Hackl, D. H. Leach, and J. J. Neumeier, Phys. Rev. Lett. **72**, 396 (1994); **72**, 3291 (1994).

[12] L. A. Falkovsky and S. Klama, Physica C **172**, 242 (1990).

[13] P. B. Allen, Phys. Rev. B **13**, 1416 (1976).

[14] S. L. Cooper and M. V. Klein, Comments Condens. Matter Phys. **15**, 19 (1990).

[15] S. L. Cooper, M. V. Klein, B. G. Pazol, J. P. Rice, and D. M. Ginsberg, Phys. Rev. B **37**, 5920 (1988); R. Hackl, in *Electronic Properties of High-T_c Superconductors and Related Compounds*, edited by H. Kuzmany, M. Mehring, and Z. Fisk, Springer Series in Solid-State Sciences Vol. 99 (Springer, Berlin, 1991).

[16] S. L. Cooper *et al.*, Phys. Rev. B **38**, 11 934 (1988); X. K. Chen *et al.*, *ibid.* **48**, 10 530 (1993), and references therein.

[17] X. K. Chen *et al.*, in Phys. Rev. Lett. **73**, 3290 (1994).

[18] R. Hackl, W. Glaser, P. Müller, D. Einzel, and K. Andres, Phys. Rev. B **38**, 7133 (1988).

[19] T. Staufer, R. Nemetschek, R. Hackl, P. Müller, and H. Veith, Phys. Rev. Lett. **68**, 1069 (1992).

[20] R. Nemetschek, O. V. Misochko, B. Stadlober, and R. Hackl, Phys. Rev. B **47**, 3450 (1993).

[21] A. Hoffmann *et al.*, Physica C **235-240**, 1897 (1994).

[22] A. A. Maksimov *et al.*, Zh. Eksp. Teor. Fiz. **97**, 1047 (1990) [Sov. Phys. JETP **70**, 588 (1990)].

[23] Important information can also be obtained from the renormalization of low-lying phonons as the gap opens below T_c [see, e.g., C. Thomsen, in *Light Scattering in Solids VI*, edited by M. Cardona and G. Güntherodt (Springer, Berlin, 1991)]. The theory of the polarization dependence of the phonon renormalization in a $d_{x^2-y^2}$ superconductor has been recently given in Ref. 46.

[24] O. Betbedet-Matibet and P. Nozieres, Ann. Phys. (N.Y.) **51**, 392 (1969).

[25] D. Vollhardt and P. Wölfle, *The Superfluid Phases of ^3He* (Taylor & Francis, London, 1990).

[26] T. Tsuneto, Phys. Rev. **118**, 1029 (1960).

[27] P. J. Hirschfeld, P. Wölfle, J. A. Sauls, D. Einzel, and W. O. Putikka, Phys. Rev. B **40**, 6695 (1989).

[28] D. Pines and P. Nozieres, *The Theory of Quantum Liquids* (Benjamin, New York, 1966).

[29] P. J. Hirschfeld and D. Einzel, Phys. Rev. B **47**, 8837 (1993).

[30] D. Einzel and C. Schuster (unpublished).

[31] T. P. Devereaux, Phys. Rev. Lett. (to be published).

[32] M. Sigrist and M. Rice, Z. Phys. B **68**, 9 (1987).

[33] See, e.g., J. Yu and A. J. Freeman, J. Phys. Chem. Solids

[34]W. E. Pickett, Rev. Mod. Phys. **61**, 433 (1989).
[35]M. Tinkham, *Group Theory and Quantum Mechanics* (McGraw-Hill, New York, 1964).
[36]M. C. Krantz and M. Cardona, Phys. Rev. Lett. **72**, 3290 (1994).
[37]H. Monien and A. Zawadowksi, Phys. Rev. Lett. **63**, 911 (1989).
[38]A. Zawadowski *et al.* (unpublished).
[39]This indicates that the energy gap can only be identified with the peak position in the B_{1g} channel, and the temperature dependence of the peak position will most closely follow its true form only in this channel. However, it is to be noted that impurities will also change the position of the peak away from $2\Delta_0$ even in this channel as well (see Refs. 10 and 31), making the identification of the gap from the peak maximum less precise.
[40]X. K. Chen *et al.*, Physica C **227**, 113 (1994) (however, screening was not taken into account in these calculations); T. P. Devereax, J. Supercond. (to be published).
[41]G. Kotliar, Phys. Rev. B **37**, 3664 (1988); R. Joynt, *ibid.* **41**, 4271 (1990); see also Q. P. Li, B. E. C. Koltenbah, and R. Joynt, *ibid.* **48**, 437 (1993).
[42]D. S. Rokhsar, Phys. Rev. Lett. **70**, 493 (1993); R. B. Laughlin, Physica C **234**, 280 (1994).
[43]S. Chakravarty, A. Sudbo, P. W. Anderson, and S. Strong, Science **261**, 337 (1993).
[44]J. C. Campuzanno (private communication).
[45]A. Virosztek and J. Ruvalds, Phys. Rev. B **45**, 347 (1992); T. Moriya *et al.*, J. Phys. Soc. Jpn. **52**, 2905 (1990); A. Sokol and D. Pines, Phys. Rev. Lett. **71**, 2813 (1993).
[46]T. P. Devereaux, A. Virosztek, and A. Zawadowski, Phys. Rev. B **51**, 505 (1995); T. P. Devereaux, *ibid.* **50**, 10 287 (1994).
[47]D. S. Hirashima and H. Namaizawa, J. Low Temp. Phys. **73**, 137 (1988).
[48]V. J. Emery, Synth. Met. **13**, 21 (1986); K. Miyake, S. Schmitt-Rink, and C. M. Varma, Phys. Rev. B **34**, 6554 (1986); D. J. Scalapino, E. Loh, and J. E. Hirsch, *ibid.* **34**, 5370 (1986); P. Monthoux, A. V. Balatsky, and D. Pines, Phys. Rev. Lett. **67**, 3449 (1991).
[49]K. Itai, Phys. Rev. B **45**, 707 (1992).